

## A Study of Finite Amplitude Barotropic Instability

HUNG-CHI KUO<sup>1</sup> and CHUNG-HO HORNG<sup>1</sup>

(Manuscript received 2 November 1993, in final form 15 May 1994)

### ABSTRACT

We report cases with a series of disturbances tilted upshear along the shear zone during the Mei-Yu season. The scale involved is much smaller than the local Rossby radius of deformation; we hypothesize the relevance of barotropic instability, and have explored the nonlinear evolution of barotropic instability. The small and finite amplitude theories are reviewed; their relevance to the observations are briefly discussed. Eigenvalues of ideal three and four region models are calculated analytically. A new Fourier Chebyshev nondivergent barotropic model is constructed. With the initial value problem approach, our experiments on barotropic instability with a vorticity strip either have hyperbolic tangent or Bicklerly jet type of wind profiles. We studied the time evolution of the shear layers in terms of the formation of fundamental eddies and successive pairing or merging of eddies. The mutual intensification of counter-propagating Rossby waves (vorticity gradient waves) across the vorticity strip, breakdown of the vorticity strip, local concentration of vorticity and vortex merging processes were simulated. While the barotropic instability is an efficient way to concentrate vorticity in a small region, the later vortex merging can enlarge the vortex sizes but not the intensity of the resultant vortex. We propose that the concentration and the merging of vortices can create a favorable localized environment within the shear zone for the moist baroclinic processes to operate.

As far as the intensity, shape and evolution of the individual vortices are concerned, they are very sensitive to initial background noise ( $1/100$  of mean vorticity). In other words, there is no predictability in the nonlinear evolution. However, the maximum growth rate and the dominant wavelength of vortex can be predicted from the linear analysis. The Bicklerly jet possesses higher growth rate than the hyperbolic tangent case on the  $f$  plane. We document chaotic behavior of sudden breakup of shear zone and associated vortex merging after a couple of regular cycles of wave-mean flow interaction with shear zone maintained. In the thirty-day integration, the vortices on the  $\beta$  plane become disorganized and scattered while they still remain well organized on the  $f$  plane.

(Key words: Barotropic instability, Vortex merging, Counter-propagating, Rossby waves)

---

<sup>1</sup> Department of Atmospheric Science, National Taiwan University, Taipei, Taiwan, R.O.C.

## 1. INTRODUCTION

Mei-Yu season in subtropical Asia is the transition period between the dry northeast and moist southwest monsoons. There have been many studies on Mei-Yu fronts and their associated phenomena (see Chen 1992 for a review). An interesting feature of the Mei-Yu season is a series of disturbances growing along the shear zones. These shear zones often extend from the surface up to 700 hPa and are associated with a weak temperature gradient over southern China (Chen and Chang, 1980). Because of the weak temperature gradient and smaller scale involved (smaller than the local Rossby radius of deformation), the significant wind change across the shear zone suggests that barotropic instability may be related to the growth of disturbances along the shear line.

Figure 1 shows the 850 hPa wind, temperature and the  $p$  velocity of 700 hPa in a 12 hour sequence starting at 12Z, May 13, 1993. The strong baroclinicity and wind shear that resemble the classical hyperbolic tangent wind profile over south China (center of the map) in this case is obvious. The scale of the shear vorticity is on the order of  $10^{-4} \text{ s}^{-1}$ . We note that the wind shear is the strongest at 12Z, May 13, and then decreases as time proceeds. Figure 2 shows the *IR* satellite picture at 00Z, May 14, which corresponds to time in Figure 1b. Figure 3 gives the 3 hour sequence of *IR* satellite pictures starting at 13Z, May 13. Figures 2 and 3 indicate that convections were best organized into a series of disturbances around 00Z, May 14, some twelve hour later than the strong wind shear of 12Z on May 13. The wavelength of the disturbance was about 300 km to 400 km. In addition, Figures 2 and 3 reveal that the disturbances around May 14, 00Z are elongated in the northeast-southwest direction, which are tilted upshear as is required by barotropic instability. Even with the presence of baroclinicity and moisture processes, the small-scale nature plus the features described seem to suggest the relevance of barotropic instability.

Another evidence of the relevance of barotropic instability can be seen from the satellite pictures on June 6, 1992 (Figure 4). In the one-hour sequence of the enhanced satellite picture starting at 07Z on June 6, we observed a series of disturbances grow and decay within a four hour period. In addition, we observed a wavy type of cloud structure surrounding the general area of interest. The synoptic condition did not change significantly during this period, thus we only show the 850 hpa observations at 12Z on June 6, 1992 (Figure 5). If we are to believe the clouds are signatures of waves or a vorticity field, not only do we see a series of disturbances in the center of the shear zone, but also a wavy structures in both the northern and southern ends of the shear zones. From these satellite images, the wavelength of these waves is about 120 km and the disturbances have a diameter of about 30 km. The ridges or troughs of the waves are north-south oriented, tilted upshear as is required by barotropic instability. In addition, these wavy cloud signatures over the edge of the shear zone are consistent with the argument of counter-propagating Rossby waves (vorticity gradient waves along both edges of a vorticity anomaly strip) interpretation of barotropic instability (Hoskins *et al.* 1985). The two cases reported here suggest the relevance (or importance) of barotropic instability. However, they do not necessarily imply that the growth of series of disturbances along the shear zone is a pure barotropic case. Certainly, moist baroclinic processes may play an important role. In this paper, we will investigate the relevance of barotropic instability in the development of these disturbances.

Conventionally, the barotropic instability of a shear flow with or without the downstream variation are studied in the linear sense. Namely, the instability is studied by either the eigenvalue-eigenvector approach or by the numerical integration technique (e.g. Kuo, 1949,

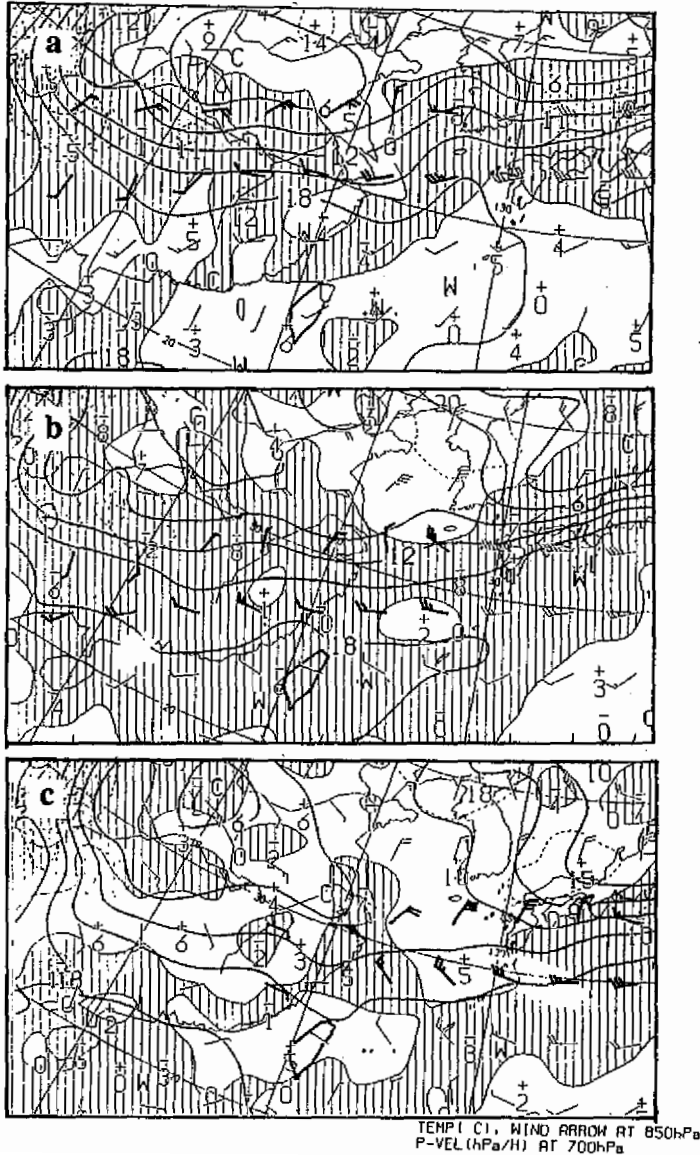


*Fig. 1.* 850 hPa wind, temperature and the  $p$  velocity of 700 hPa in a 12 hour sequence. (a) is at 12Z, May 13, 1993, (b) 00Z, May 14, and (c) 12Z, May 14. Hatched area indicates upward motion region.

Crum and Stevens, 1990, among many others). In both approaches, the growth rate and most unstable structure are emphasized. In addition to the review given in Crum and Stevens (1990), more references on barotropic instability can be found in the recent work of Sun and Chang (1992). They apply the numerical integration technique to the hyperbolic type of shear with downstream variation, with the application to Mei-Yu fronto-cyclogenesis in mind. They also emphasized the predictability of linear stability. In this paper, we take the initial value problem approach, with the inviscid nonlinear evolution in our mind. Thus,

1993-05-14 00:32Z IR LCC

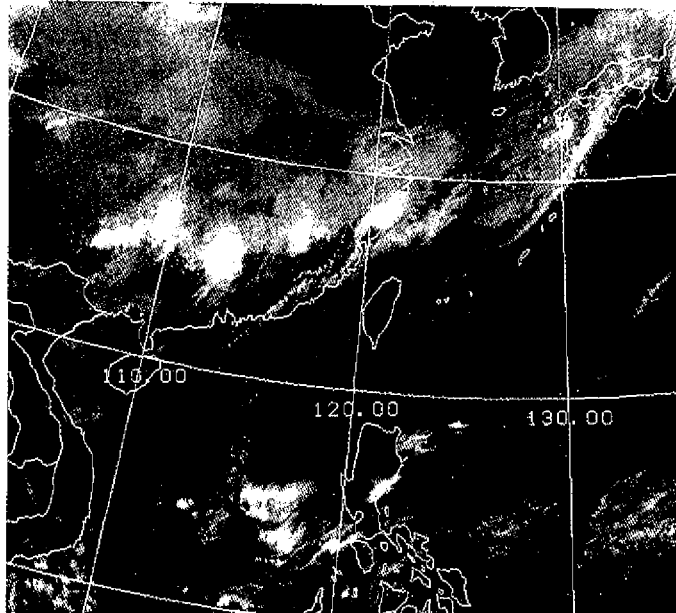


Fig. 2. IR satellite picture at 00Z, May 14, 1993, corresponding to time in Figure 1b.

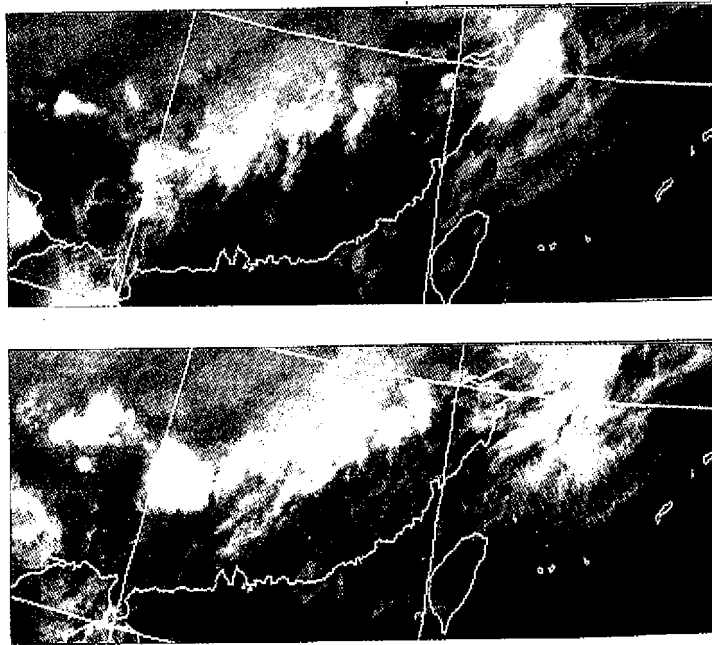
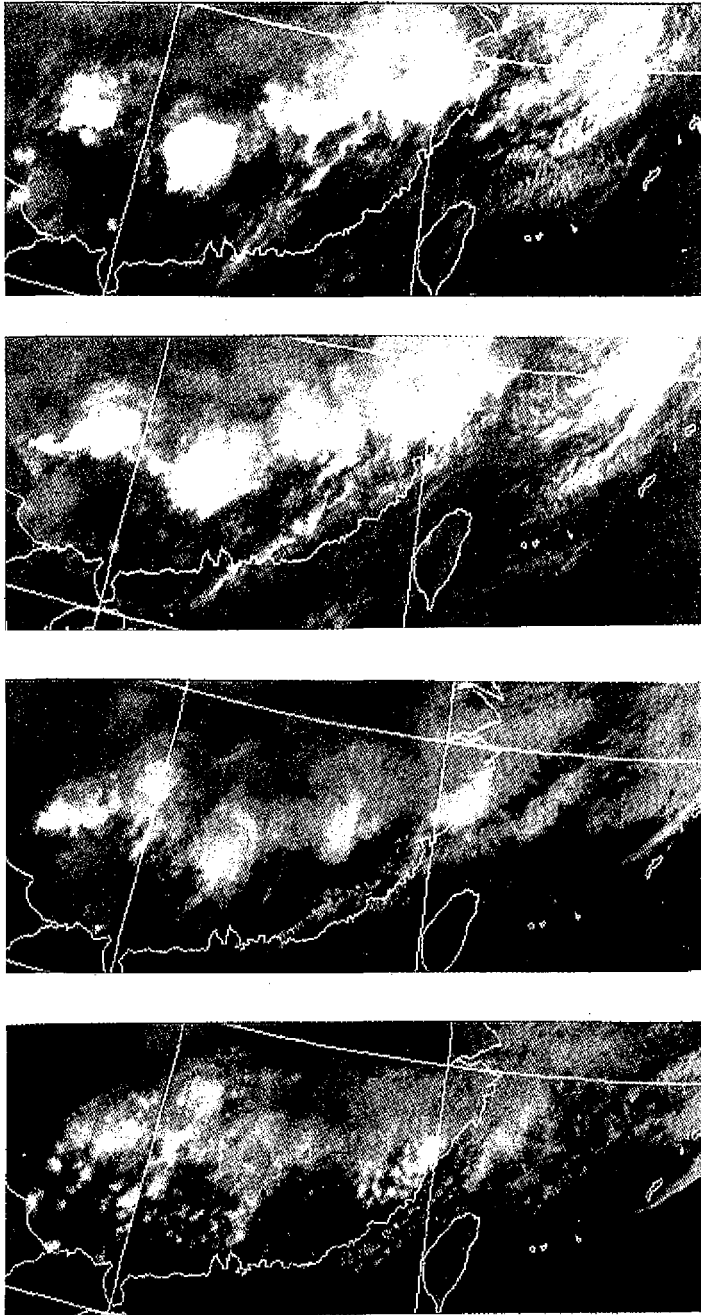
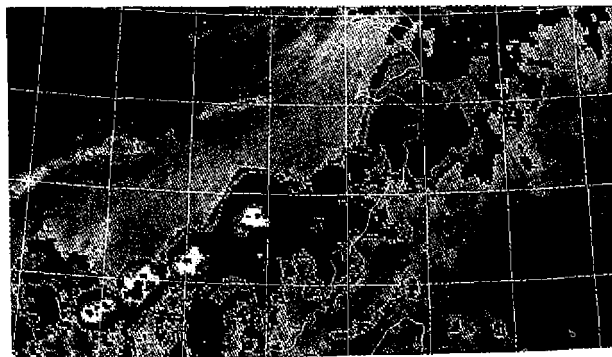
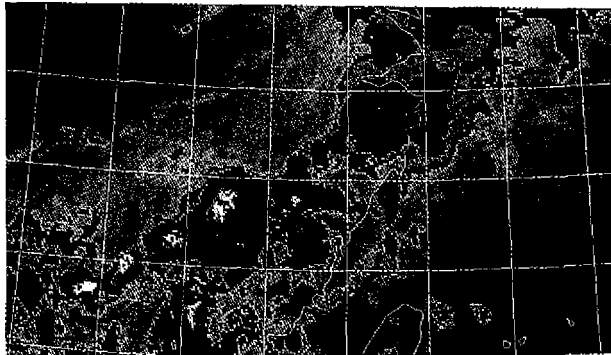
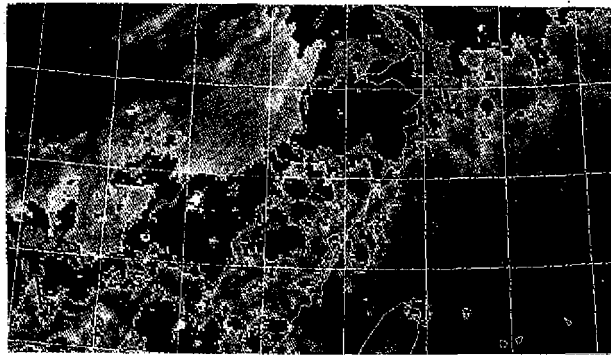


Fig. 3. 3 hour sequence of IR satellite pictures starting at 13Z, May 13, 1993.



*Fig. 3. (Continued.)*



*Fig. 4.* Enhanced satellite pictures in the one hour sequence starting at 07Z, June 6, 1992.

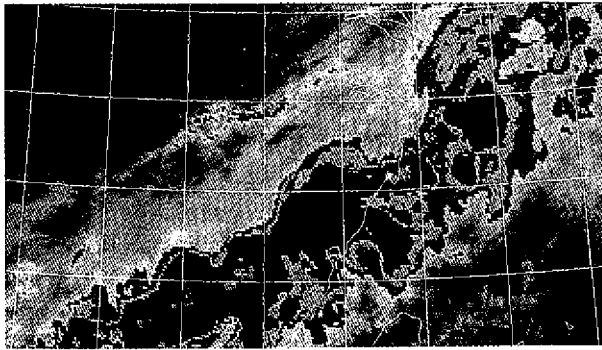
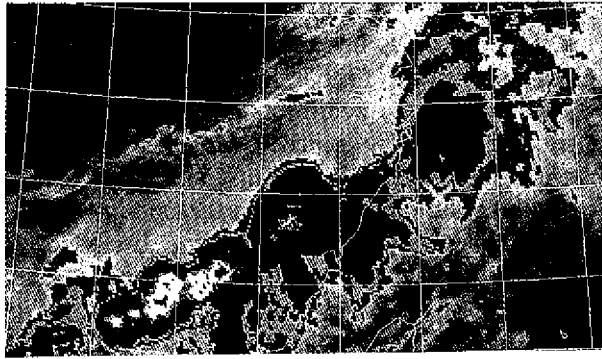


Fig. 4. (Continued.)

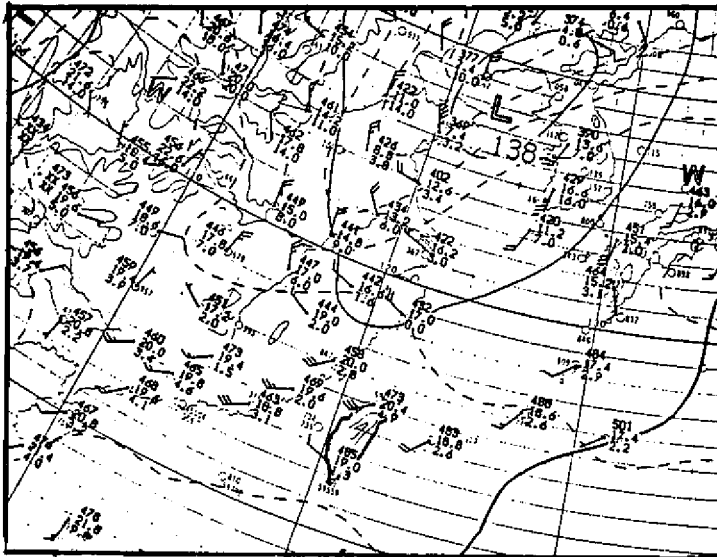


Fig. 5. 850 hPa observations at 12Z, June 6, 1992.

our approach is different also from Williams *et al.* (1984). They studied the nonlinear effects of barotropic instability in a downstream varying easterly jet. To study the long term equilibrium in their model, frictional effect is included in their mean forcings. Similar to Lesieur *et al.* (1988), we explore the nonlinear time evolution of shear zone in terms of the formation of fundamental eddies and successive pairing and merging of eddies. Unlike Lesieur *et al.* (1988), our calculation is inviscid and includes the Bickerly jet type of shear flow. Moreover, we emphasize the predictability in the nonlinear evolution. Simulations of chaotic breakdown of shear zones are also performed and discussed. A new spectral Fourier Chebyshev nondivergent barotropic model, which conserves mean enstrophy and mean kinetic energy, was built for that purpose.

In section 2 we perform analytical calculations of eigenvalue of ideal three and four region models. In addition, we review the theories (linear and nonlinear) of barotropic instability and their relevance to observations are also briefly discussed. The Fourier Chebyshev spectral barotropic model is formulated in section 3. The nonlinear evolution of shear zones in terms of eddies interaction is given in section 4. Section 5 summarizes the results and gives concluding remarks.

## 2. NONDIVERGENT AND DIVERGENT BAROTROPIC INSTABILITY THEORIES

Before we study finite amplitude barotropic instability *numerically*, we review non-divergent, divergent, linear and nonlinear barotropic instability theories. In addition, we perform linear analysis (eigenvalue and eigenvector approach) of three-region (hyperbolic tangent) and four-region (Bickerly jet) models analytically. The sufficient condition for non-divergent linear stability, which can be found in many dynamic textbooks, is included for the completeness of the review and comparison for the finite amplitude theory.

### 2.1 Sufficient Condition for Nondivergent Linear Stability

We consider the nondivergent vorticity equation linearized about a basic state zonal state  $\bar{u}$  which is a function of  $y$  only. The linearized equation takes the form

$$\frac{\partial \zeta'}{\partial t} + \bar{u} \frac{\partial \zeta'}{\partial x} + v' \frac{d\bar{\zeta}}{dy} = 0, \quad (2.1)$$

where

$$\bar{\zeta} = f - \frac{\partial \bar{u}}{\partial y}, \zeta' = \frac{\partial v'}{\partial x} - \frac{\partial u'}{\partial y}, \quad (2.2a, b)$$

$f$  is Coriolis parameter and the perturbation wind components  $(u', v')$  satisfy the nondivergent relation

$$\frac{\partial u'}{\partial x} + \frac{\partial v'}{\partial y} = 0. \quad (2.3)$$

Defining  $D/Dt$  as the derivative following the basic state zonal flow, the first two terms in (2.1) can be written as  $D\zeta'/Dt$ . Defining the meridional particle displacement  $\eta$  by  $D\eta/Dt = v'$ , we integrate (2.1) to obtain

$$\zeta' + \eta \frac{d\bar{\zeta}}{dy} = 0. \quad (2.4)$$

Multiplying (2.4) by  $v'$  leads to

$$\frac{DA}{Dt} = -v'\zeta', \quad (2.5a)$$

where

$$A = \frac{d\bar{\zeta}}{dy} \frac{1}{2} \eta^2 = \left(\frac{d\bar{\zeta}}{dy}\right)^{-1} \frac{1}{2} \zeta'^2, \quad (2.5b)$$

is the wave-activity (Andrews *et al.*, 1987). While there is a phase variable, whose time and space derivatives are interpreted as the local frequency and wavenumber, the wave-activity governs the wave intensity. It is the conservation of linear and nonlinear wave-activity we shall derive.

Using (2.2b) and the condition of nondivergence in the right hand side of (2.5a), we now write the conservation of wave-activity

$$\frac{\partial A}{\partial t} + \frac{\partial[\bar{u}A + \frac{1}{2}(v'^2 - u'^2)]}{\partial x} + \frac{\partial[-u'v']}{\partial y} = 0. \quad (2.6)$$

Integration of (2.6) over the domain with vanishing activities along the boundary yields

$$\frac{d}{dt} \int \int A dx dy = 0. \quad (2.7)$$

Since the integral in (2.7) must be time invariant, (2.5b) shows that if  $\bar{\zeta}$  is a monotonically increasing function of  $y$ , neither  $\eta^2$  nor  $\zeta'^2$  can grow in an overall sense. Thus, a necessary condition for instability is that  $d\bar{\zeta}/dy$  have both signs. As has discussed Eliassen (1983) that a frequent wording of this condition, namely that the vorticity gradient vanishes somewhere within the domain, is inexact; for one thing,  $d\bar{\zeta}/dy$  does not have to be everywhere a continuous function of  $y$ .

The above argument has been generalized in several ways. Baroclinic effects can be included in both quasigeostrophic (Charney and Stern 1962) and semigeostrophic (Eliassen 1983, Magnusdottir and Schubert 1990, 1991) frameworks. Moreover, the analysis need not be limited to parallel shear flow (Andrews, 1983) or even to linear dynamics (Arnol'd 1965, 1966; Drazin and Reid 1981; McIntyre and Shepherd 1987; Shepherd 1988a,b, 1989). We shall consider the nonlinear extension now.

## 2.2 Sufficient Condition for Nondivergent Nonlinear Stability

To generalize the linear arguments of the previous subsection, we now consider the nonlinear nondivergent barotropic equation

$$\frac{\partial \zeta}{\partial t} + u \frac{\partial \zeta}{\partial x} + v \frac{d\zeta}{dy} = 0, \quad (2.8)$$

where

$$\zeta = f + \frac{\partial v}{\partial x} - \frac{\partial u}{\partial y} \quad (2.9)$$

is the absolute vorticity and the wind components  $(u, v)$  satisfy the continuity equation

$$\frac{\partial u}{\partial x} + \frac{\partial v}{\partial y} = 0. \quad (2.10)$$

We divide the fields into a basic state part and a part associated with wave or eddies, e.g.,  $\zeta(x, y, t) = \bar{\zeta}(y) + \zeta'(x, y, t)$ , where the primed variables are departures from the basic state, and are not necessary small amplitude. The  $x$  invariant basic state flow is assumed to be a steady solution of (2.8). We consider the case in which  $\bar{\zeta}(y)$  is a monotonically increasing function of  $y$ , and thereby define the inverse function  $\bar{y}(\zeta)$  such that  $\bar{y}(\bar{\zeta}(y)) = y$ . Differentiating this last expression yields  $\bar{y}_\zeta \bar{\zeta}_y = 1$ .

As the nonlinear generalization of the small amplitude wave-activity (2.5b), we now follow McIntyre and Shepherd (1987), Shepherd (1988a), Haynes (1988) and Schubert *et al.* (1992) to define

$$A(\bar{\zeta}, \zeta') = \int_0^{\zeta'} [\bar{y}(\bar{\zeta} + \tilde{\zeta}) - \bar{y}(\bar{\zeta})] d\tilde{\zeta}. \quad (2.11)$$

By approximating  $\bar{y}(\bar{\zeta} + \tilde{\zeta})$  the first two terms in Taylor series expansion about  $\bar{\zeta}$ , (2.11) reduces to (2.5b). To derive the equation of  $A(\bar{\zeta}, \zeta')$  we first take the total derivative of this finite amplitude wave-activity to obtain

$$\frac{DA}{Dt} = \frac{\partial A}{\partial \bar{\zeta}} \frac{D\bar{\zeta}}{Dt} + \frac{\partial A}{\partial \zeta'} \frac{D\zeta'}{Dt}, \quad (2.12)$$

where, from (2.11),

$$\frac{\partial A}{\partial \bar{\zeta}} = \bar{y}(\bar{\zeta} + \zeta') - \bar{y}(\bar{\zeta}) - \bar{y}_\zeta(\bar{\zeta})\zeta', \quad (2.13)$$

$$\frac{\partial A}{\partial \zeta'} = \bar{y}(\bar{\zeta} + \zeta') - \bar{y}(\bar{\zeta}). \quad (2.14)$$

Equations (2.13) and (2.14), together with the fact that  $-D\zeta'/Dt = D\bar{\zeta}/Dt = v'd\bar{\zeta}/dy$ , allow (2.12) to be written as

$$\frac{DA}{Dt} = -v'\zeta', \quad (2.15)$$

which is a nonlinear generalization of (2.5a). Using the nondivergent condition (2.10), we can write down counterparts of (2.6), the finite amplitude wave-activity conservation equation

$$\frac{\partial A}{\partial t} + \frac{\partial[uA + \frac{1}{2}(v'^2 - u'^2)]}{\partial x} + \frac{\partial[vA - u'v']}{\partial y} = 0. \tag{2.16}$$

By comparing (2.6) and (2.16), several differences are noteworthy. All the primed quantities in (2.6) are small amplitude, whereas the primed quantities in (2.16) may be of finite amplitude. Where the flux  $(uA, vA)$  appears in the finite amplitude relation (2.16), the flux  $(\bar{u}A, 0)$  appears in the small-amplitude relation (2.6).

To obtain the nonlinear stability condition, we integrate (2.16) over the domain to yield

$$\frac{d}{dt} \int \int A dx dy = 0. \tag{2.17}$$

Although (2.17) looks identical to (2.7), the integrand  $A$  in (2.17) is defined by (2.11), while the  $A$  in (2.7) is defined by (2.5b). The results are consistent since (2.11) reduces to (2.5b) in the small amplitude limit. From (2.11) one should note that

$$\int_0^{\zeta'} \left| \frac{d\bar{y}}{d\bar{\zeta}} \right|_{min} \tilde{\zeta} d\tilde{\zeta} \leq |A| \leq \int_0^{\zeta'} \left| \frac{d\bar{y}}{d\bar{\zeta}} \right|_{max} \tilde{\zeta} d\tilde{\zeta},$$

and thus

$$\frac{\frac{1}{2}\zeta'^2}{|\bar{\zeta}_{\bar{y}}|_{max}} \leq |A| \leq \frac{\frac{1}{2}\zeta'^2}{|\bar{\zeta}_{\bar{y}}|_{min}}. \tag{2.18}$$

Together, (2.17) and (2.18) imply that

$$\begin{aligned} & \frac{1}{2|\bar{\zeta}_{\bar{y}}|_{max}} \int \int \zeta'^2(x, y, t) dx dy \leq \int \int A(\bar{\zeta}, \zeta', t) dx dy \\ & = \int \int A(\bar{\zeta}, \zeta', 0) dx dy \leq \frac{1}{2|\bar{\zeta}_{\bar{y}}|_{min}} \int \int \zeta'^2(x, y, 0) dx dy, \end{aligned}$$

which can also be written

$$\int \int \zeta'^2(x, y, t) dx dy \leq \frac{|\bar{\zeta}_{\bar{y}}|_{max}}{|\bar{\zeta}_{\bar{y}}|_{min}} \int \int \zeta'^2(x, y, 0) dx dy. \tag{2.19}$$

This is the form of Arnol'd's (1965, 1966) result derived by McIntyre and Shepherd (1987) and used by Shepherd (1988a) to obtain rigorous bounds on the nonlinear saturation of barotropic instabilities to parallel shear flows. The inequality (2.19) bounds the disturbance enstrophy at time  $t$  in terms of the initial disturbance enstrophy and the northward gradient of the basic state absolute vorticity.

### 2.3 Linear Analysis of Three and Four Region Model

To confirm that a zonal flow is unstable and to find the growth rates and modes of breakdown of the flow, an eigenvalue-eigenfunction calculation is useful. Following the

classical approach of Rayleigh (1945, pages 392-394), Gill (1982), Haurwitz (1949) and Guinn and Schubert (1993), let us consider the nondivergent barotropic model on an infinite  $f$  plane. For a basic state shear defined by

$$\bar{u} = \begin{cases} 0 & y_0 \leq y < \infty; \\ \zeta_0(y - y_0) & 0 \leq y \leq y_0; \\ -\zeta_0(y + y_0) & -y_0 \leq y \leq 0; \\ 0 & -\infty < y \leq -y_0, \end{cases} \quad (2.20)$$

and the corresponding relative vorticity is

$$\bar{\zeta}(y) = -\frac{d\bar{u}}{dy} = \begin{cases} 0 & y_0 \leq y < \infty; \\ -\zeta_0 & 0 \leq y \leq y_0; \\ \zeta_0 & -y_0 \leq y \leq 0; \\ 0 & -\infty < y \leq -y_0, \end{cases} \quad (2.21)$$

where  $\zeta_0$  and  $y_0$  are constant. The  $\bar{u}$  is a four region idealization of the so called "Bickerly jet" ( $-\zeta_0 y_0 \operatorname{sech}^2(y/y_0)$ ). The  $\bar{u}$  and  $\bar{\zeta}$  of this model are shown in Figure 6a. Now consider the linearized nondivergent barotropic vorticity equation

$$\left(\frac{\partial}{\partial t} + \bar{u} \frac{\partial}{\partial x}\right) \nabla^2 \psi + \frac{d\bar{\zeta}}{dy} \frac{\partial \psi}{\partial x} = 0, \quad (2.22)$$

where  $\psi$  is the streamfunction for the perturbation winds  $u' = -\partial\psi/\partial y$  and  $v' = \partial\psi/\partial x$ , in which cases the  $\zeta' = \nabla^2\psi$ . We shall search for the solution of (2.22) with the basic state of (2.20). Assuming the solution has the form  $\psi(x, y, t) = \sum_{kc} \Psi_{kc}(y) e^{ik(x-ct)}$  where  $k$  is the real zonal wavenumber,  $c$  is the phase speed which can be a complex. Dropping the subscript  $kc$  of  $\Psi_{kc}(y)$  for simplicity and performing the discrete Fourier transform to (2.22) yields

$$\frac{d^2\Psi}{dy^2} + \left(\frac{\bar{\zeta}_y}{\bar{u} - c} - k^2\right)\Psi = 0. \quad (2.23)$$

Since the basic vorticity  $\bar{\zeta}$  is piecewise constant, the perturbation vorticity will vanish everywhere except along the line  $y = 0$  and  $y = \pm y_0$ . As solutions of (2.22) which are bounded as  $|y| \rightarrow \infty$ , we have

$$\Psi(y) = \Psi_s e^{-k|y+y_0|} + \Psi_m e^{-k|y|} + \Psi_n e^{-k|y-y_0|}, \quad (2.24a)$$

or

$$\psi(x, y, t) = \sum_{kc} (\Psi_s e^{-k|y+y_0|} + \Psi_m e^{-k|y|} + \Psi_n e^{-k|y-y_0|}) e^{ik(x-ct)}, \quad (2.24b)$$

where  $\Psi_n$ ,  $\Psi_m$  and  $\Psi_s$  are complex constants. The solution associated with the constant  $\Psi_m$  has vorticity anomaly concentrated in  $y = 0$  and the corresponding stream function

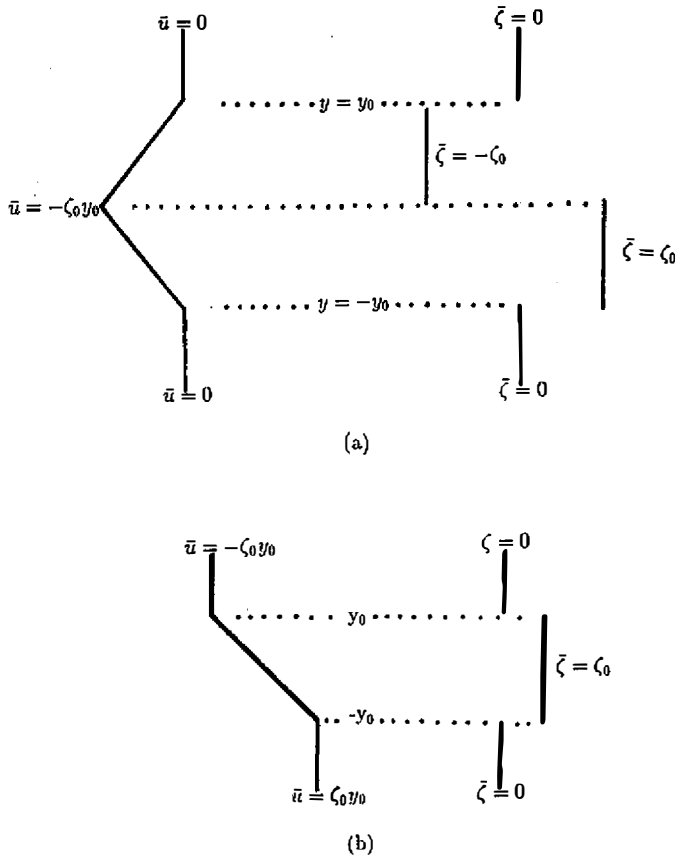


Fig. 6.  $y$  profiles of  $\bar{u}$  and  $\bar{\zeta}$  in the ideal four region (easterly Bickerly jet) (3.a) and in the ideal three region (hyperbolic tangent shear) (3.b).

decays when it is away from  $y = 0$ . Similarly, the solution associated with the constants  $\Psi_n$  ( $\Psi_s$ ) has vorticity concentrated in  $y = y_0$  ( $y = -y_0$ ) and the corresponding stream function decay away from  $y = y_0$  ( $y = -y_0$ ). To determine  $\Psi_n$ ,  $\Psi_m$  and  $\Psi_s$ , we integrate (2.23) over a narrow region centered on either  $y = 0$  or  $y = \pm y_0$  and let the narrow region approach zero. This yields

$$(\bar{u} - c)\Delta \frac{d\Psi}{dy} + \Psi\Delta\bar{\zeta} = 0 \quad \text{at } y = 0, \pm y_0, \tag{2.25}$$

where  $\Delta$  stands for the jump across the narrow region. Substituting (2.24) into (2.25), we obtain

$$(2\sigma + 1)\Psi_n + e^{-\mu}\Psi_m + e^{-2\mu}\Psi_s = 0, \tag{2.26}$$

$$e^{-\mu}\Psi_n + (1 - \mu - \sigma)\Psi_m + e^{-\mu}\Psi_s = 0, \tag{2.27}$$

$$e^{-2\mu}\Psi_n + e^{-\mu}\Psi_m + (2\sigma + 1)\Psi_s = 0, \tag{2.28}$$

where  $\mu = ky_0$  is the dimensionless wave number and  $\sigma = kc/\zeta_0$  the dimensionless growth rate or frequency. If the basic state vorticity jumps at the middle and southern interface were removed, the last two terms in (2.26) would disappear and the vorticity gradient (Rossby) wave on the northern interface would propagate with phase speed  $c = c_n$  where  $c_n = -\zeta_0 y_0 / 2ky_0$ . Similarly, if the basic state vorticity jumps at the middle and northern interface were removed, (2.27) indicates the Rossby wave (vorticity gradient wave) on the southern interface propagate with the phase speed  $c = c_s$  where  $c_s = -\zeta_0 y_0 / 2ky_0$ . Finally, removing the jumps in both northern and southern interfaces yield a Rossby phase speed  $c = c_m$  where  $c_m = -\zeta_0 y_0 + \zeta_0 y_0 / ky_0$ . The system (2.26)–(2.28) can be regarded as a concise mathematical description of the interaction of three counter-propagating Rossby waves (vorticity gradient waves). The second term in (2.26) gives the effect of the middle vorticity anomaly pattern on the behavior of the northern vorticity anomaly while the third term in (2.26) gives the effect of the southern vorticity anomaly pattern on the behavior of the northern vorticity anomaly. Similar argument can also be applied to (2.27) and (2.28). Note that the effect of these interactions decays with increasing wave number and increasing shear layer width according to the exponential decay.

Regarding (2.26)–(2.28) as a linear homogeneous system with unknowns  $\Psi_n, \Psi_m$  and  $\Psi_s$ , we require that the determinant of the coefficients vanish, which yields the cubic equation

$$\sigma^3 + \mu\sigma^2 + \left(\mu - \frac{3}{4} - \frac{e^{-4\mu}}{4} + e^{-2\mu}\right)\sigma + \frac{1}{4}(\mu - 1 - e^{-4\mu} - \mu e^{-4\mu} + 2e^{-2\mu}) = 0. \tag{2.29}$$

The dimensionless growth rate  $\sigma$  as a function of  $\mu$  computed from (2.29) is shown in Figure 7. Also plotted in Figure 7 is the dimensionless growth rate for the three region model we shall now discuss.

The basic state shear for the three region model considered is defined by

$$\bar{u} = \begin{cases} -\zeta_0 y_0 & y_0 \leq y < \infty; \\ -\zeta_0 y & -y_0 \leq y \leq y_0; \\ \zeta_0 y_0 & -\infty < y \leq -y_0, \end{cases} \tag{2.30}$$

and the corresponding relative vorticity is

$$\bar{\zeta}(y) = -\frac{d\bar{u}}{dy} = \begin{cases} 0 & y_0 \leq y < \infty; \\ \zeta_0 & -y_0 \leq y \leq y_0; \\ 0 & -\infty < y \leq -y_0, \end{cases} \tag{2.31}$$

where  $\zeta_0$  and  $y_0$  are constant. The  $\bar{u}$  is a three region idealization of hyperbolic tangent basic flow ( $\bar{u} = -\zeta_0 y_0 \tanh(y/y_0)$ ). The  $\bar{u}$  and  $\bar{\zeta}$  of this model are shown in Figure 6b. As have discussed in Guinn and Schubert (1993), and identical to the approach of the four region model, we have the dimensionless growth rate

$$\sigma = \pm \frac{1}{2} [(1 - 2\mu)^2 - e^{-4\mu}]^{\frac{1}{2}}. \tag{2.32}$$

Note that the unstable mode occurs in the three region model if  $0 \leq ky_0 \leq 0.6392$  and in the four region model if  $0 \leq ky_0 \leq 1.8291$ . The peak instability for the three region

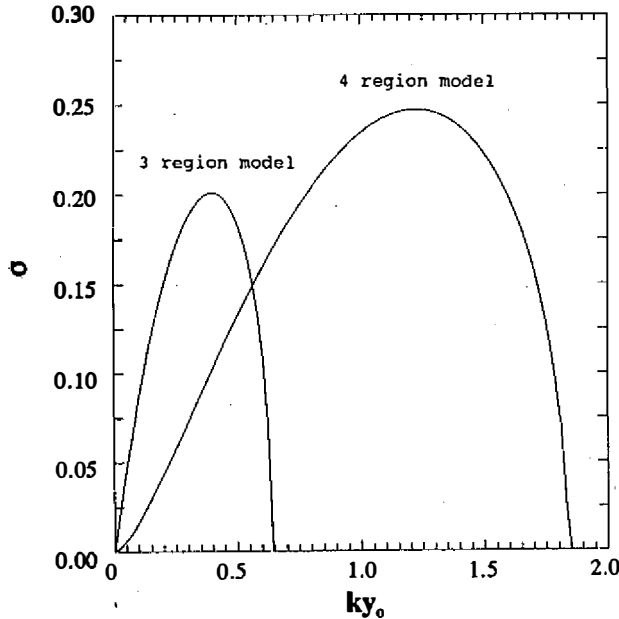


Fig. 7. Dimensionless growth rate as a function of dimensionless wavenumber for the three and four region model. The unstable mode occurrence in a three region model within  $0 \leq ky_0 \leq 0.6392$  and in a four region model within  $0 \leq ky_0 \leq 1.8291$ .

model occurs at  $ky_0 = 0.3984$ , which corresponds to a zonal wave length approximately seven or eight times the width of the strip. The most unstable mode in the four region model occurs at  $ky_0 = 1.2261$ , which corresponds to a zonal wave length approximately four times the width of the strip. In the most unstable mode in the three region hyperbolic tangent type of model the time behavior is  $e^{0.2012\zeta_0 t}$ , so the  $e$ -folding time is approximately  $5 / \zeta_0$ . Since the vorticity is on the order of  $10^{-4} \text{ s}^{-1}$  on the cases reported in this paper, the  $e$ -folding time requires only a couple of hours, which is consistent with the satellite pictures in Figure 3. On the other hand, the most unstable mode in the four region Bickerly jet type of model is  $e^{0.2470\zeta_0 t}$ , so the  $e$ -folding time is approximately  $4 / \zeta_0$ . In summary, the analysis here indicates that “Bickerly jet” possesses a greater range of instability in wave number space than the “hyperbolic tangent” case, and is more unstable than the “hyperbolic tangent” case.

### 2.4 Sufficient Condition for Divergent Linear Stability

Some of the nondivergent barotropic instability theorems of the previous subsection can be generalized to the divergent barotropic model and to discretely layered (but not continuously stratified) primitive equation model (thus no quasigeostrophic assumption required) on the  $\beta$ -plane and sphere (Ripa 1983, 1991). Considering the following shallow water equation

$$\frac{\partial u'}{\partial t} + \bar{u} \frac{\partial u'}{\partial x} + v' \frac{d\bar{u}}{dy} - f v' + g \frac{\partial h'}{\partial x} = 0, \tag{2.33}$$

$$\frac{\partial v'}{\partial t} + \bar{u} \frac{\partial v'}{\partial x} + f u' + g \frac{\partial h'}{\partial y} = 0, \tag{2.34}$$

$$\frac{\partial h'}{\partial t} + \bar{u} \frac{\partial h'}{\partial x} + v' \frac{d\bar{h}}{dy} + \bar{h} \left( \frac{\partial u'}{\partial x} + \frac{\partial v'}{\partial y} \right) = 0, \quad (2.35)$$

where the primed variables denote small perturbations about a purely zonal basic flow,  $\bar{u}$  associated depth  $\bar{h}$ . To derived Ripa's theorem we need to combine (2.33)–(2.35) into equations for

$$E' = \frac{1}{2} [\bar{h}(u'^2 + v'^2) + 2\bar{u}u'h' + gh'^2], \quad (2.36)$$

$$M' = h'u', \quad (2.37)$$

$$P' = \frac{1}{\bar{h}} \left( \frac{\partial v'}{\partial x} - \frac{\partial u'}{\partial y} - \bar{P}h' \right), \quad (2.38)$$

where  $\bar{P} = (f - \frac{d\bar{u}}{dy})/\bar{h}$ , the basic state potential vorticity.

The  $E'$  equation can be derived by  $(\bar{h}u' + \bar{u}h') \cdot (2.33) + (\bar{h}v' \cdot (2.34) + (\bar{u}u' + gh') \cdot (2.35))$ , which has the form

$$\frac{\partial E'}{\partial t} + \bar{h}^2 \bar{u} P' v' + \frac{\partial}{\partial x} [(\bar{u}u' + gh')(\bar{h}u' + h'\bar{u})] + \frac{\partial}{\partial y} [(\bar{u}u' + gh')\bar{h}v'] = 0. \quad (2.39)$$

The  $M'$  equation can be derived by  $h' \cdot (2.33) + u' \cdot (2.35)$ ,

$$\frac{\partial M'}{\partial t} + \bar{h}^2 P' v' + \frac{\partial}{\partial x} [u'M' + \frac{1}{2}(gh'^2 + u'^2 - v'^2)] + \frac{\partial}{\partial y} [\bar{h}u'v'] = 0. \quad (2.40)$$

The equation for  $P'$ , obtained by forming the vorticity equation from (2.33)–(2.34) and then eliminating the divergence using (2.35), takes the form

$$\frac{\mathcal{D}P'}{\mathcal{D}t} + \frac{d\bar{P}}{dy} v' = 0, \quad (2.41)$$

where  $\mathcal{D}/\mathcal{D}t$  is the same operator as used in (2.5a). Again, defining the meridional particle displacement  $\eta$  by  $\mathcal{D}\eta/\mathcal{D}t = v'$ , we can integrate (2.41) to obtain

$$P' + \frac{d\bar{P}}{dy} \eta = 0, \quad (2.42)$$

which is a generalization of (2.4). Multiplication of (2.42) by  $v'$  yields

$$P'v' + \frac{\mathcal{D}}{\mathcal{D}t} \left( \frac{d\bar{P}}{dy} \frac{1}{2} \eta^2 \right) = 0. \tag{2.43}$$

Integrating (2.39) and (2.40) over the domain gives

$$\int \int \left( \frac{\partial E'}{\partial t} + \bar{h}^2 \bar{u} P'v' \right) dx dy = 0, \tag{2.44}$$

and

$$\int \int \left( \frac{\partial M'}{\partial t} + \bar{h}^2 P'v' \right) dx dy = 0. \tag{2.45}$$

Multiplying (2.45) by the constant  $u_0$ , then subtracting (2.44) and using (2.43) for  $P'v'$  lead to

$$\frac{d}{dt} \int \int \left[ E' - u_0 M' + \bar{h}^2 \frac{d\bar{P}}{dy} (u_0 - u) \frac{\eta^2}{2} \right] dx dy = 0, \tag{2.46}$$

which is the divergent barotropic generalization of the nondivergent barotropic result (2.7). We now argue that if  $E' - u_0 M' \geq 0$  and  $(u_0 - u) d\bar{P}/dy \geq 0$ , (2.46) does not allow  $\eta^2$  to grow in an overall sense. Since  $E' - u_0 M' \geq 0$  if  $(u_0 - u)^2 \leq g\bar{h}$ , we now state Ripa's generalization of the theorems of Rayleigh and Fjortoft. *If there exists any value of  $u_0$  such that*

$$(u_0 - u) \frac{d\bar{P}}{dy} \geq 0 \quad \text{and} \quad (u_0 - u)^2 \leq g\bar{h} \tag{2.47a, b}$$

for all  $y$ , then the flow is stable to infinitesimal perturbations. Ripa has also discussed several corollaries of (2.47), one of which is obtained by choosing  $u_0 = \max[\bar{u}]$ . This results in the following weaker sufficient condition for stability. *If*

$$\frac{d\bar{P}}{dy} \geq 0 \quad \text{and} \quad \max[\bar{u}] \leq \min[\bar{u} + (g\bar{h})^{\frac{1}{2}}] \tag{2.48a, b}$$

for all  $y$ , then the flow is stable to infinitesimal perturbations.

To recover the stability results for the nondivergent barotropic model from the stability results for the shallow water model we consider the limit  $g\bar{h} \rightarrow \infty$ , in which (2.47b) are satisfied for any finite  $u_0$ . Then, there is no difference between the  $\bar{P}$  and  $\bar{\zeta}$ , and a choice of  $u_0$  such that  $u_0 - u < 0$  everywhere leads to  $d\bar{\zeta}/dy \leq 0$  everywhere as sufficient for stability, while the choice of  $u_0$  such that  $u_0 - u > 0$  everywhere leads to  $d\bar{\zeta}/dy \geq 0$  everywhere as sufficient for stability. Therefore, a necessary condition for instability is that  $d\bar{\zeta}/dy$  have both signs (Rayleigh's theorem). If  $d\bar{\zeta}/dy = 0$  at  $y = \tilde{y}$  and choosing  $u_0 = \bar{u}(\tilde{y})$  leads from (2.47a) to  $(\bar{u}(\tilde{y}) - \bar{u}(y)) d\bar{\zeta}/dy < 0$  everywhere as a necessary condition for instability (Fjortoft's theorem). The Fjortoft theorem implies that the relative background flow and the vorticity gradient are positively correlated. Namely, the vorticity

gradient waves are propagating against the relative background flow in such a way that phase-locking is possible.

Finally we note that, unlike the nondivergent barotropic model, in application of shallow water stability theory to atmospheric data or to the interpretation of atmospheric models with continuous stratification there is a considerable freedom in the choice of mean depth, and reasonable  $\bar{h}$ 's should probably exceed 100 m. Calculations from Schubert *et al.* (1992) in their Australian summer monsoon study, in consistent with (2.47), indicates that a deeper  $\bar{h}$  allows a faster growth rate for barotropic instability. The horizontal wind shear zones often extend from surface up to 700 hPa during the Mei-Yu season, which will give a not too small  $\bar{h}$  (second or third vertical internal mode). However, the growth rate will be smaller than the estimation from the nondivergent barotropic model.

### 3. THE SPECTRAL NONDIVERGENT BAROTROPIC VORTICITY EQUATION

The starting point for our numerical model is the nondivergent barotropic vorticity equation in a periodic  $\beta$  channel. Because we are interested in internal dynamics depending only on the initial basic wind profile, a periodic channel is used instead of an open boundary condition. Since the flow is constrained to be nondivergent, we can write these equations in the vorticity/streamfunction form

$$\left\{ \begin{array}{l} \frac{\partial^2 \psi}{\partial x^2} + \frac{\partial^2 \psi}{\partial y^2} = \zeta \\ \psi(x, 0, t) = \psi(x, H, t) = 0 \end{array} \right\}, \quad (3.1)$$

$$\frac{\partial \zeta}{\partial t} + \frac{\partial}{\partial x} \left( -\frac{\partial \psi}{\partial y} \zeta \right) + \frac{\partial}{\partial y} \left( \frac{\partial \psi}{\partial x} \zeta \right) + \beta \frac{\partial \psi}{\partial x} = 0. \quad (3.2)$$

This is a closed system in  $\psi$  and  $\zeta$ , where  $\psi$  and  $\zeta$  are the streamfunction and vorticity and  $\beta$  is the gradient of Coriolis parameter  $f$ . We shall solve (3.1)–(3.2) on the domain  $0 \leq x \leq L$ ,  $0 \leq y \leq H$ , with the assumption that all variables are periodic in  $x$  and  $\psi = 0$  on  $y = 0, H$ . In the following we discuss an accurate spectral method (Fourier-Chebyshev tau method) for solving the system (3.1)–(3.2).

The simulation of barotropic instability places great demands on spatial discretization schemes used in simulation models. In the present work we have used a spectral scheme in both horizontal directions. In the  $x$  direction, Fourier basis functions are used so that the periodicity is built into each basis function. In the  $y$  direction, Chebyshev polynomial basis functions are used; the north and south boundary conditions are not satisfied by each basis function, but rather by the series as a whole.

The dependent variables  $\psi$  and  $\zeta$  are approximated by the series expansions

$$\begin{bmatrix} \psi(x, y, t) \\ \zeta(x, y, t) \end{bmatrix} = \sum_{m=-M}^M \sum_{n=0}^N \begin{bmatrix} \hat{\psi}_{mn}(t) \\ \hat{\zeta}_{mn}(t) \end{bmatrix} T_n(y') e^{2\pi i m x / L}, \quad (3.3)$$

where the  $T_n(y')$  are the Chebyshev polynomials defined on the interval  $-1 \leq y' \leq 1$  by  $T_n(y') = \cos(n\phi)$  with  $y' = 2y/H - 1 = \cos \phi$ . Let us define the Fourier-Chebyshev inner product of two functions  $f(x, y)$  and  $g(x, y)$  as

$$\langle f, g \rangle = \frac{1}{L} \int_{-1}^1 \int_0^L \frac{f(x, y)g^*(x, y)}{(1 - y'^2)^{1/2}} dx dy' , \tag{3.4}$$

where the star denotes complex conjugate. The spectral coefficient  $\hat{\psi}_{mn}(t)$  is given by

$$\hat{\psi}_{mn}(t) = \frac{2}{\pi c_n} \left\langle \psi(x, y, t), T_n(y')e^{2\pi imx/L} \right\rangle \tag{3.5}$$

with  $c_n = \begin{cases} 2 & n=0 \\ 1 & n>0 \end{cases}$ . Similar relations hold for  $\hat{\zeta}_{mn}(t)$ . Equation (3.5) is the transform from physical space to Fourier-Chebyshev spectral space and (3.3) is the inverse transform.

The coefficients in (3.3) are determined by requiring the residual in (3.2) to be orthogonal to all the basis functions  $T_n(y')e^{2\pi imx/L}$  ( $-M \leq m \leq M$  and  $0 \leq n \leq N$ ), the residual in the Poisson equation (3.1) to be orthogonal to all the basis functions except those for which  $n = N - 1, N$ , and the boundary conditions on  $\psi$  to be satisfied by the series as a whole. Thus, with the nonlinear terms defined by

$$A = -\frac{\partial\psi}{\partial y}\zeta, \quad B = \frac{\partial\psi}{\partial x}\zeta , \tag{3.6}$$

the tau equations are

$$\left\{ \begin{array}{l} \frac{4}{H^2 c_n} \sum_{\substack{p=n+2 \\ p+n \text{ even}}}^N p(p^2 - n^2)\hat{\psi}_{mp} - \left(\frac{2\pi m}{L}\right)^2 \hat{\psi}_{mn} = \hat{\zeta}_{mn} \quad (n = 0, 1, 2, \dots, N-2) \\ \sum_{p=0}^N (-1)^p \hat{\psi}_{mp} = 0 \\ \sum_{p=0}^N \hat{\psi}_{mp} = 0 \end{array} \right\} , \tag{3.7}$$

$$\frac{d\hat{\zeta}_{mn}}{dt} + \hat{A}_{mn}^{(1,0)} + \hat{B}_{mn}^{(0,1)} + \beta\hat{\psi}_{mn}^{(1,0)} = 0 , \tag{3.8}$$

where  $\hat{A}_{mn}^{(1,0)}$  is the spectral coefficient of  $\partial A/\partial x$  and  $\hat{B}_{mn}^{(0,1)}$  is the spectral coefficient of  $\partial B/\partial y$ . Some of the details in the derivation of (3.7)–(3.8) are given in Kuo and Schubert (1988). The relation between  $\hat{A}_{mn}^{(1,0)}$  and  $\hat{A}_{mn}$  (the spectral coefficient of  $A$ ) is

$$\hat{A}_{mn}^{(1,0)} = i \left( \frac{2\pi m}{L} \right) \hat{A}_{mn} , \tag{3.9}$$

while the relation between  $\hat{B}_{mn}^{(0,1)}$  and  $\hat{B}_{mn}$  (the spectral coefficient of  $B$ ) is

$$\hat{B}_{mn}^{(0,1)} = \frac{4}{Hc_n} \sum_{\substack{p=n+1 \\ p+n \text{ odd}}}^N p \hat{B}_{mp}. \quad (3.10)$$

Although the spectral evaluation of  $y$  derivatives by (3.10) looks at first sight more difficult than the spectral evaluation of  $x$  derivatives by (31), we find that this is not the case. Equation (3.10) yields the (backward) recurrence formula

$$c_{n-1} \hat{B}_{m,n-1}^{(0,1)} - \hat{B}_{m,n+1}^{(0,1)} = \frac{4}{H} n \hat{B}_{m,n} \quad (n = 1, 2, \dots, N-1) \quad (3.11)$$

with the starting values  $\hat{B}_{m,N+1}^{(0,1)} = \hat{B}_{m,N}^{(0,1)} = 0$ . For fixed  $m$ , the use of (3.11) allows the  $N$  values of  $\hat{B}_{mn}^{(0,1)}$  to be computed in  $O(N)$  operations. The transform method (Orszag, 1970; Eliassen *et al.*, 1970) is used in computing the spectral coefficients  $\hat{A}_{mn}$  and  $\hat{B}_{mn}$ . To eliminate aliasing error in the quadratic nonlinear terms,  $3M$  points in  $x$  and  $3N/2$  points in  $y$  are needed in the physical domain.

In the numerical time integration of the above equations, we must solve (3.7) at each time step. For a given  $m$  ( $-M \leq m \leq M$ ), we regard (3.7) as a linear algebraic system in the  $N+1$  unknowns  $\hat{\psi}_{mn}$  ( $0 \leq n \leq N$ ), with known right hand side  $\hat{\zeta}_{mn}$ . The matrix structure of this linear system is upper triangular except for the last two rows, which come from the boundary conditions. There are many possible ways to solve (3.7), two of which are discussed by Gottlieb and Orszag (1977, page 119–120). Because (3.7) holds for each  $m$  separately, the direct method is a reasonable alternative, a situation which does not exist when Chebyshev expansions are used in both directions.

Using simple model equations, Fulton and Schubert (1987) have investigated the relative merits of various time differencing schemes for Chebyshev spectral methods. When the time step is limited by accuracy rather than stability (as is apparently the case here), fourth-order schemes are more efficient than second-order schemes. Fulton and Schubert have found the fourth-order Runge-Kutta scheme to be the most useful as a general rule, and it has been used here for the time integration of (3.8).

#### 4. NONLINEAR REGIME BY NUMERICAL SIMULATIONS

For the integrations presented here we have chosen the model domain to be 4500 km in both  $x$  (periodic) and  $y$  directions. In the spectral discretization we have chosen  $N = 32$  and  $M = 16$ . The transform grid for the calculation of nonlinear terms consists of 48 equally spaced points in the  $x$  direction and 48 unequally spaced points in the  $y$  direction, giving an approximate resolution of nearly 90 km in each direction. A half-hour time step is used in the fourth-order Runge-Kutta time integration. This half-hour time step retains the full accuracy of the spatial discretization. No smoothing or filtering of any kind has been used in the model. The calculations are all inviscid.

### 4.1 Hyperbolic Tangent Wind Shear Experiment

The initial condition used here is

$$\bar{u} = -u_0 \tanh\left(\frac{y}{y_0}\right) \tag{4.1}$$

where  $u_0 = 10 \text{ ms}^{-1}$  and  $y_0 = 150 \text{ km}$ . Figure 8 gives the mean vorticity and the associated wind field in physical space. The vorticity is on the order of  $10^{-4} \text{ s}^{-1}$ . The westerly to the north and easterly to the south resembles a monsoon trough or Mei-Yu front. The wind profile of Eq. (4.1) satisfied the necessary condition of barotropic instability discussed in section 2.

To initiate the instability, we have added white noise in vorticity according to DEC workstation random number set 79, with magnitude 1/100 of the initial mean vorticity field. Figure 9 gives vorticity in physical space on the  $f$ -plane simulation from day 5 to day 11. The breakdown of a vorticity strip into a pair of eddies of different size is clearly seen. According to the linear analysis in section 2, the most unstable mode has wavelength about seven or eight times the shear zone; this is consistent with our simulation. Before the formation of eddies, such as in day 7, the counter-propagating Rossby waves (vorticity gradient waves) near strip edge are obvious. In addition, the phase is oriented in the upshear sense (northeast to southwest directions). After the formation of eddies, we see that the vorticity is concentrated in a localized region. The maximum strength in the smaller eddy in day 9 is about 41 % stronger than the original mean background vorticity. The concentration of vorticity

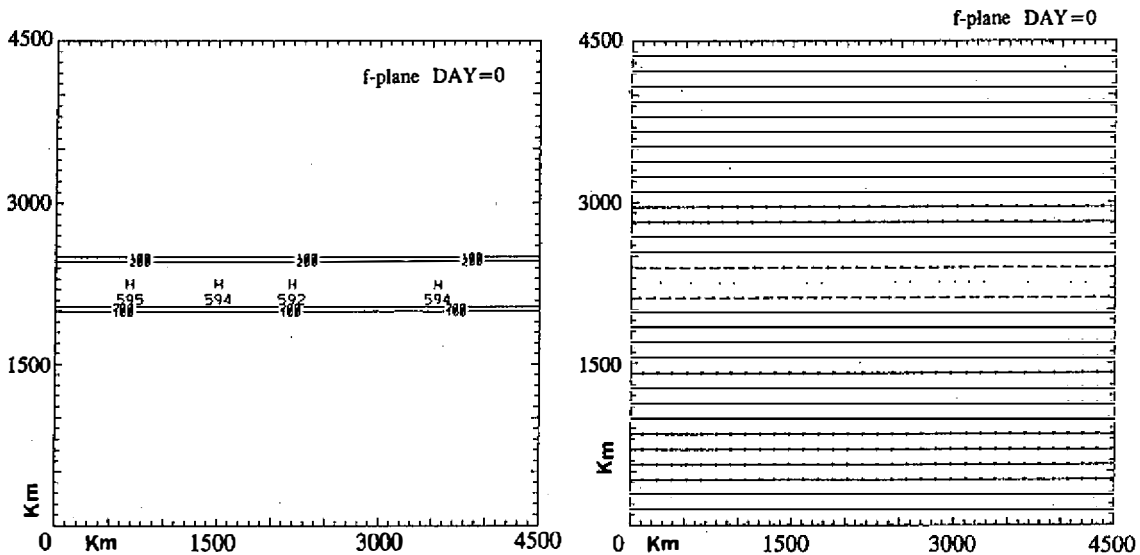


Fig. 8. Vorticity and the associated wind field in physical space. The initial condition used here is  $\bar{u} = -u_0 \tanh(y/y_0)$  where  $u_0 = 10 \text{ ms}^{-1}$  and  $y_0 = 150 \text{ km}$ . The westerly aloft and easterly below resembles a monsoon trough or Mei-Yu front. Contours of vorticity in the unit of  $10^{-7} \text{ s}^{-1}$ .

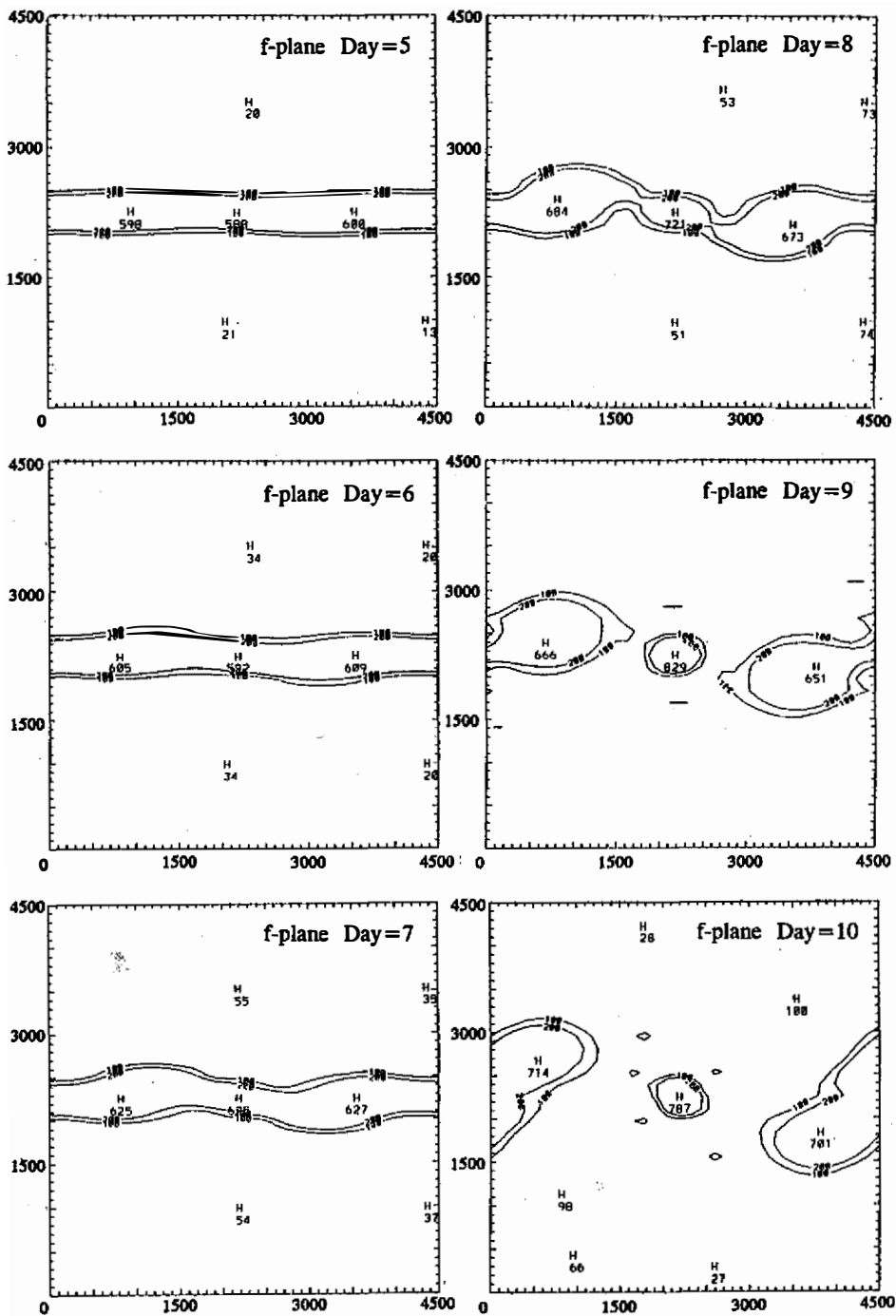


Fig. 9. Evolution of vorticity in physical space from day 5 to day 10 at one day intervals with the initial condition of Figure 8 plus  $1/100$  magnitude white noise from the random number set 79. Contours of vorticity in the unit of  $10^{-7} \text{ s}^{-1}$ .

occurs during the process of shear zone breakup. The later vortex merging will only affect the size of eddies but not the strength. Although our model cannot include the moisture physics, the local concentration of vorticity and the later vortex size merging (enlarging) processes certainly will provide a favorable background for the CISK mechanism to operate, as is in the case of typhoon (Schubert and Hack, 1982).

Note here that the formation of eddies in 7 days comes from the fact that 4500 km domain is used in the simulation. If the same  $10^{-4} \text{ s}^{-1}$  order of vorticity field is used in a 450 km domain, which is more relevant to the observational spatial scale cited in section 1, it will take 0.7 day for the eddies to grow. This is consistent with the satellite images of Figures 2-4. Figure 10 is the same as Figure 9 except the random-number set 13 is used instead. The counter-propagating vorticity gradient waves as well as the formation of vortex pairs is clearly seen. However, the time evolution is different from Figure 9. We have also performed calculations with random number set 73 and 59. Figure 11 gives the time series (up to day 30) of  $y$ -averaged spectral coefficients from wavenumber 1 to 5 for the four experiments mentioned above. We observed the dominance of wave number 1 and 2 in the time series. This reflects a pair of vortices of uneven size. This is in agreement with the satellite image (Figure 2) in which disturbances along the shear zone are of different sizes. The dominant wave number comes from the fact of our choice of computational domain and the size of shear zone. Namely, the 4500 km domain plus the 300 km shear zone allow only two most unstable waves to grow.

As revealed in Figure 11, the strength of the pair vortex go through a couple cycles, with period ranging from 4 to 6 days. Similar cycles are observed as in Figure 11. This indicates the importance of the orientation of eddies against the mean flow. Namely, the wave-mean flow interaction is crucial in the vortex evolution within the barotropic context.

Another evidence of the importance of orientation can be found in the  $f$  plane experiment with initial noise specified as  $1.0 \times 10^{-6} \cos[(i+1)2\pi/24]s^{-1} \tanh(y/y_0)$ , where  $i$  is the grid index in the  $x$  direction. This noise has the structure of wavenumber 2 with wavelength, which resembles the most unstable mode (but not the structure). Figure 12 gives the time evolution of vorticity from day 2 to day 24 with a 2 day interval. On days 4, 12, 20 we observed the upshear tilt of counter-propagating vorticity gradient waves and the follow up eddy growth. On the other hand, on days 8 and 16 we see the downshear tilt and the follow up mean flow growth. The period of the evolution is about 8 days. Figure 13 gives the vorticity field from day 25 to 30. After 3 cycles of wave-mean flow energy exchange without breaking up the shear zone, Figure 13 indicates the sudden shear zone breakup into the regime similar to Figures 9 and 10. Figure 14 gives the time series of the  $y$ -averaged spectral coefficients and the energy conversion term  $-\overline{u'v'} d\bar{u}/dy$ . The sudden breakup of the shear zone after three cycles of wave-mean flow energy exchange is obvious. Together with the case of Figure 11, this simulation suggests that the breakup of shear zones by barotropic instability can be unpredictable and chaotic.

To further explore this chaotic behavior, we perform another experiment with two initial elliptical shapes of vortex superimposed on Eq.(4.1). Figure 15 gives the vorticity field in the physical space for the chaotic experiment on  $f$  plane from day 0 to day 17 with one day interval. No white noise has been added in this experiment. Figure 16 is the same as Figure 15 except for day 24 to 40 with one day interval. Figures 15 and 16 reveal that the wave-mean flow interaction is with the rotation of the elliptical shape eddies. When the eddies rotate to the orientation that is upshear (downshear), we see the growth (weaken) of



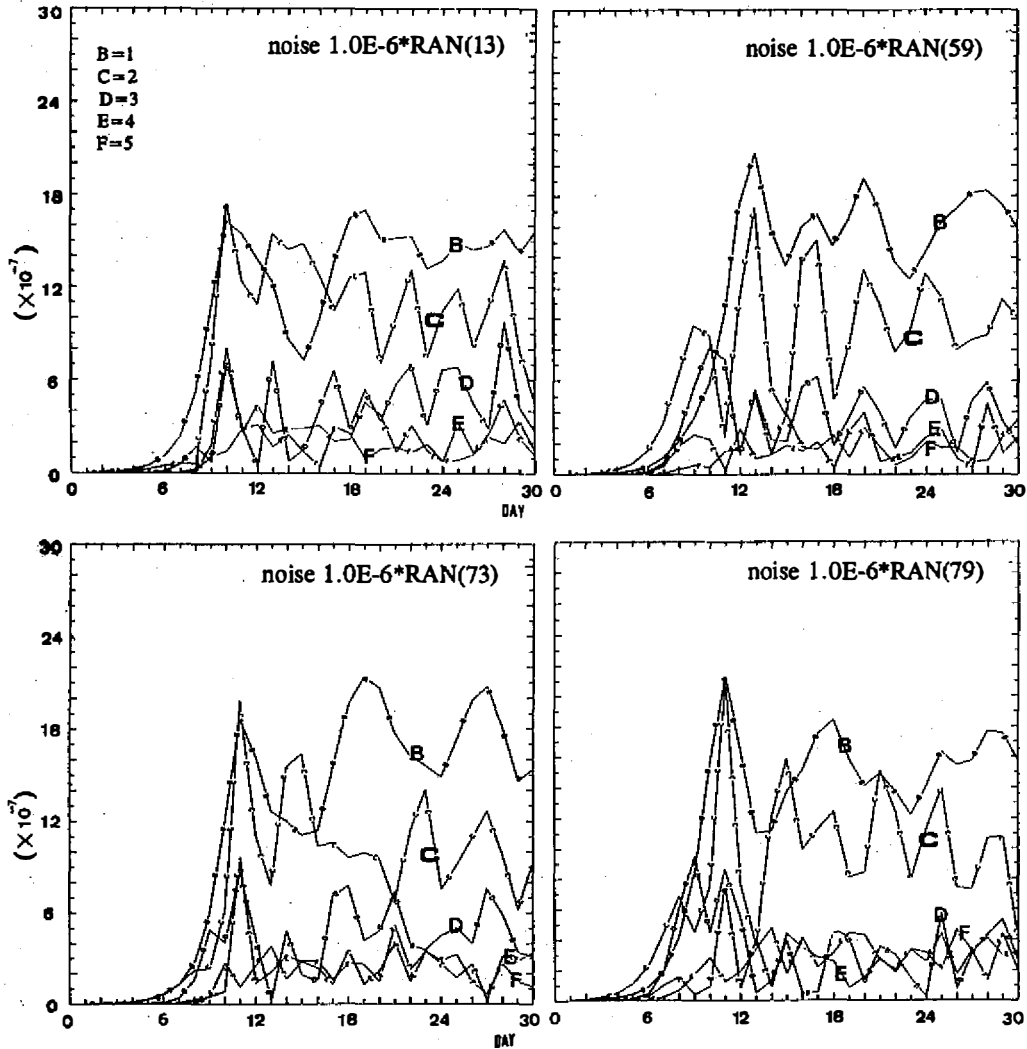
tanh profile at  $f$ -plane

Fig. 11. Time series (up to day 30) of  $y$  averaged spectral coefficients from wavenumber 1 to 5 for the four experiments with different white noise. The dominance of wave number 1 and 2 in the time series reflects a pair of vortices of uneven size.

the eddies. Figure 17 gives the time series of the  $y$ -averaged spectral coefficients. Similar to Figure 14, we observe the chaotic behavior of sudden breakup of shear zone and associated vortex merging after a very regular four cycles of wave-mean flow interaction with shear zone maintained.

We have also performed tests on the  $\beta$  plane. The  $\beta$  effect is not relevant to the observations cited in section 1. The  $\beta$ -plane calculations are used as a comparison to the  $f$ -plane result. The results, similar to the  $f$ -plane calculations in the initial period, are thus not shown here. However, there are differences in the long term behavior. Figure

18 gives the vorticity field in physical space in days 29 and 30 on  $f$  and  $\beta$  planes with random number set 13. The dominance of wave number 1 on  $f$  plane is clearly seen. However, small region vortices scattered in northwest-southeast directions on the  $\beta$ -plane result. We have also performed our test with higher resolutions and different domain sizes, the results are qualitatively similar. However, the detail time evolution is different case by case; again confirming our hypothesis that we do not have predictability on the position, shape and intensity of the eddies. They can be quite chaotic. On the other hand, the dominant wavelength of disturbances in all cases is well expected from the linear analysis. Since Figures 12-17 suggest the importance of eddies orientation against mean flow, the role of non-modal growth, optimal excitation and diagnostics of wave activities will be studied further in the future.

#### 4.2 Bickerly Jet Experiment

The initial condition used here is the easterly jet that satisfies the necessary condition discussed in section 2

$$\bar{u} = -u_0 \operatorname{sech}^2\left(\frac{y}{y_0}\right) + \frac{1}{H} \int_0^H u_0 \operatorname{sech}^2\left(\frac{y}{y_0}\right) dy \quad (4.2)$$

where  $u_0 = 10 \text{ m s}^{-1}$  and  $y_0 = 150 \text{ km}$ .

To initiate the instability, we have added white noise to the mean vorticity. Figure 19 gives vorticity in physical space on days 0, 30 and from day 3 to 12. The initial shear zone consists of strips of negative vorticity (to the north) and positive vorticity (to the south). The vorticity strip broke down into three pairs of eddies with positive and negative vorticity during day 5 to day 7. According to the linear analysis the most unstable eddy has a wavelength about four times the shear zone, which is consistent with our simulation. Before the formation of eddies, such as in day 5, the counter-propagating Rossby waves (vorticity gradient waves) with upshear tilting (northwest to southeast tilt for negative vorticity stripe and northeast to southwest for positive vorticity stripe) are obvious. After the breakup of the shear zone, we see that the local concentration of vorticity was up to 58% stronger in day 7 ( $0.93 \times 10^{-4} \text{ s}^{-1}$  to the initial background vorticity  $0.59 \times 10^{-4} \text{ s}^{-1}$ ), and up to 97% from day 8 and day 11 ( $1.12 \times 10^{-4} \text{ s}^{-1}$ ). The vorticity concentration is stronger than the hyperbolic tangent case. This agrees well with our linear analysis in section 2. Namely, the growth rate in the Bickerly jet is stronger than in the hyperbolic tangent case. Finally, we note that the vortex merging process in the simulation is different from the hyperbolic tangent case. On day 30, we have two pairs of positive and negative vorticity vortex distributed in space in a seemingly random fashion. Figure 20 is the same as Figure 19 except for the  $\beta$  plane experiment. The  $\beta$ -plane experiment gives a very similar picture to the  $f$ -plane experiment for the first 12 days. However, the long term behavior of the  $\beta$ -plane experiment contains small region vortices scattered in a seeming random fashion (day 30). Figure 21 gives the time series (up to day 30) of  $y$ -averaged spectral coefficients from wavenumber 1 to 5 for experiments with different white noises on the  $f$  plane (left column) and  $\beta$  plane (right column). After the initial dominance of wave number 3 or 4, as expected from the linear analysis, the later nonlinear regime is different case by case. No predictability for the instability seems to be an obvious conclusion.

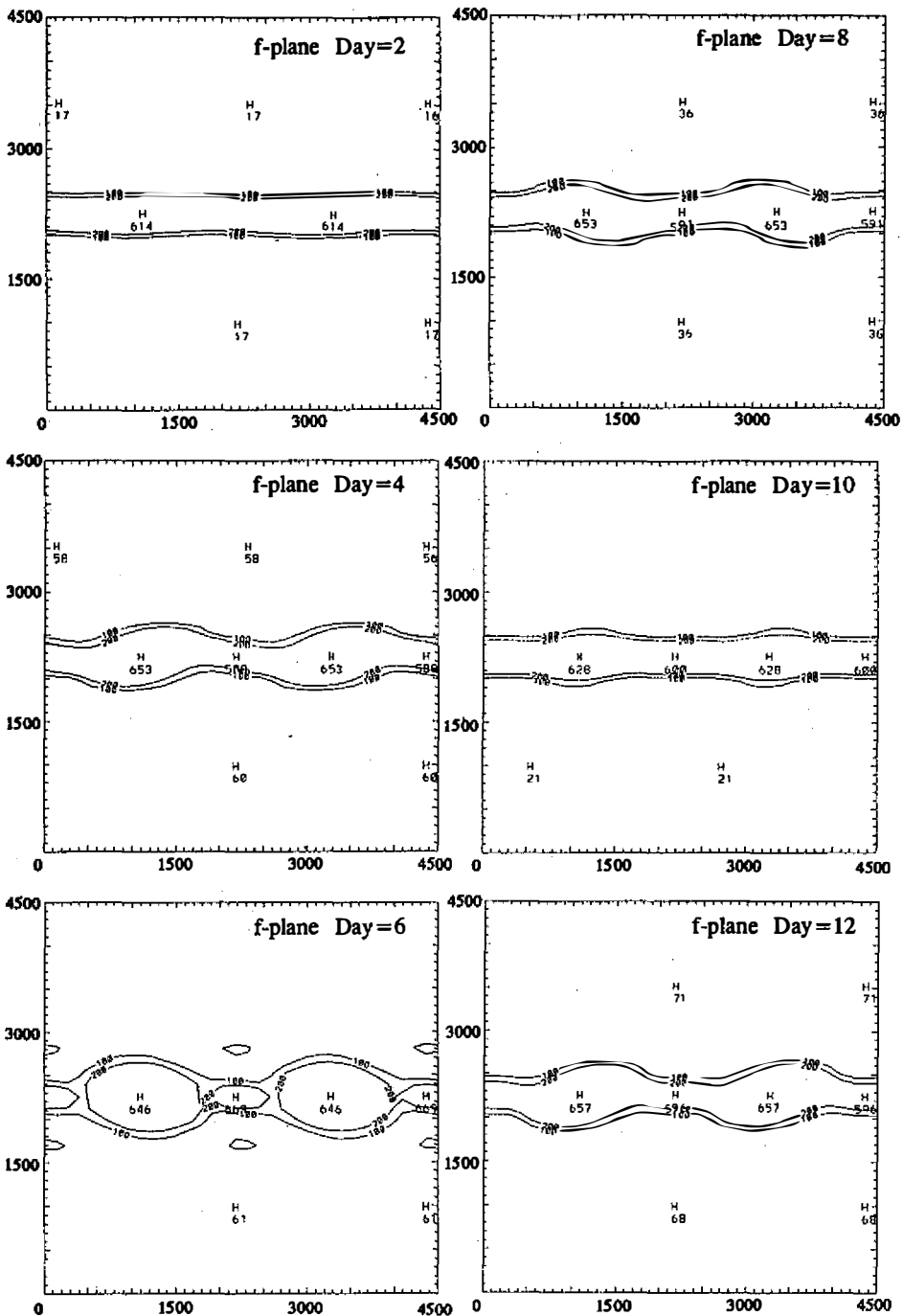


Fig. 12. Same initial condition as Figure 8 with the initial noise  $1.0 \times 10^{-6} \cos[(i+1) 2 \pi / 24] s^{-1} \tanh(y/y_0)$ , where  $i$  is the grid index in the  $x$  direction. This noise has the structure of wavenumber 2 with wavelength resembling the most unstable mode (but not the structure). The evolutions of vorticity from day 2 to day 24 with a 2-day interval are shown.

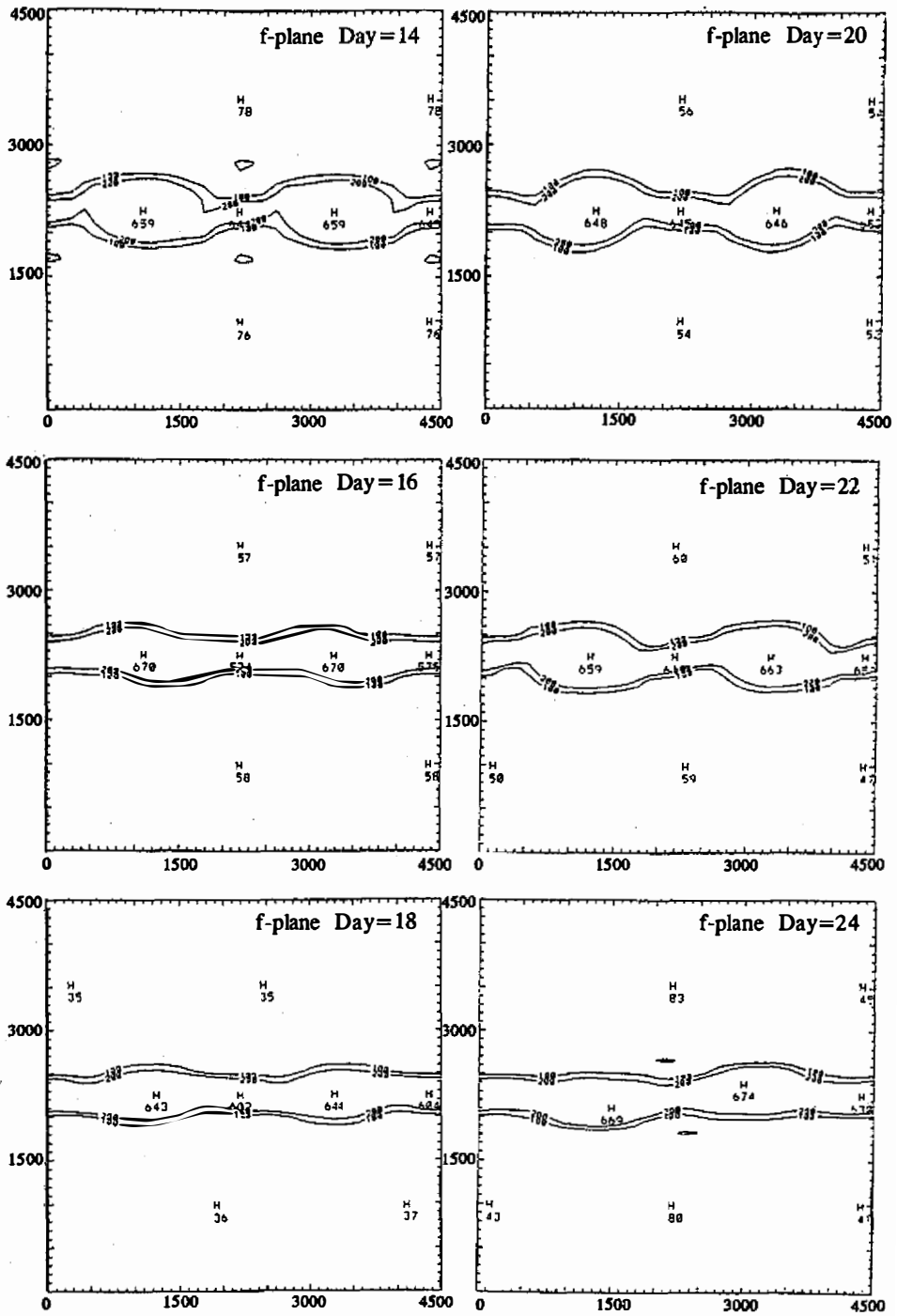


Fig. 12. (Continued.)

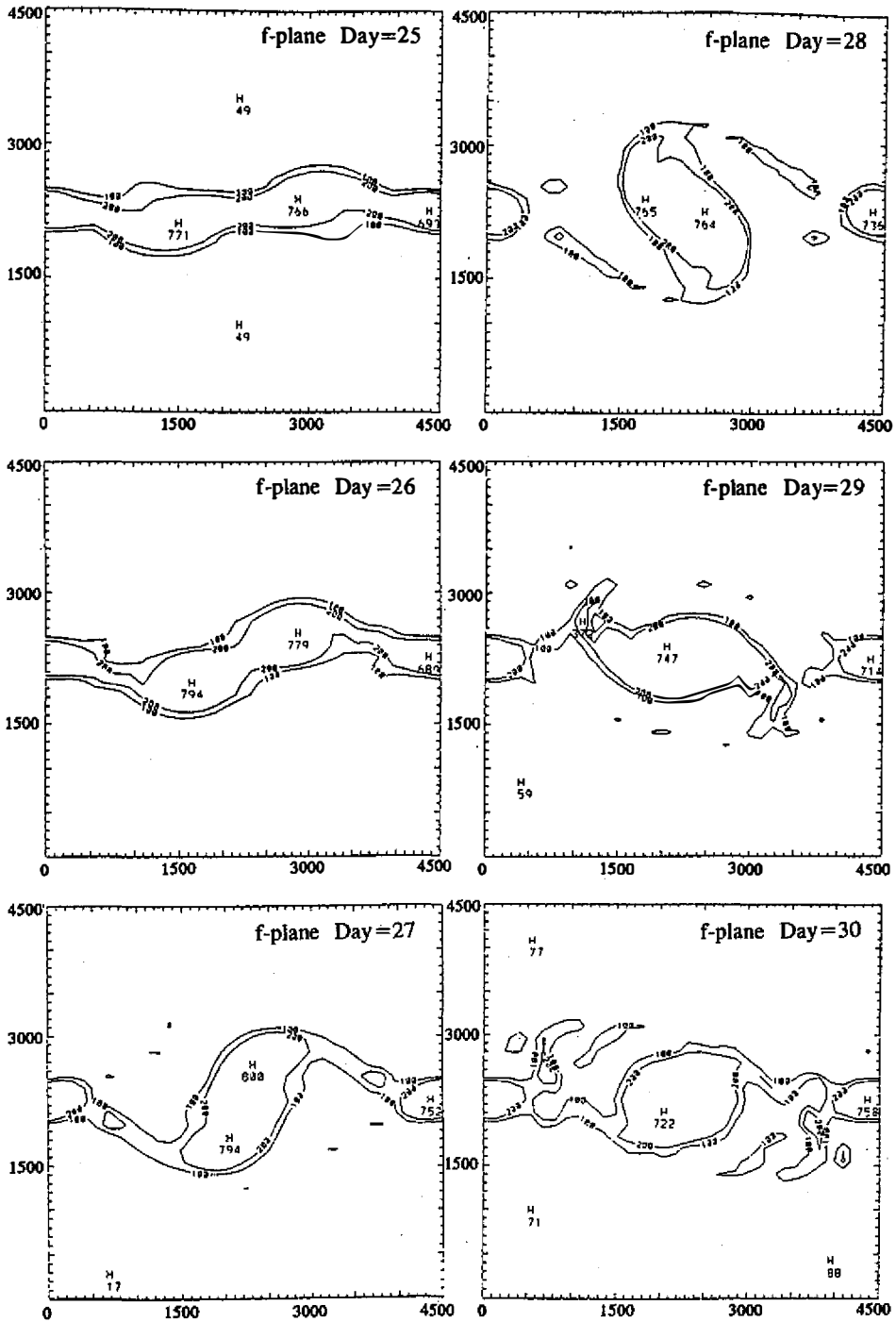


Fig. 13. Same as Figure 12 except for day 25 to day 30 with a one-day interval.

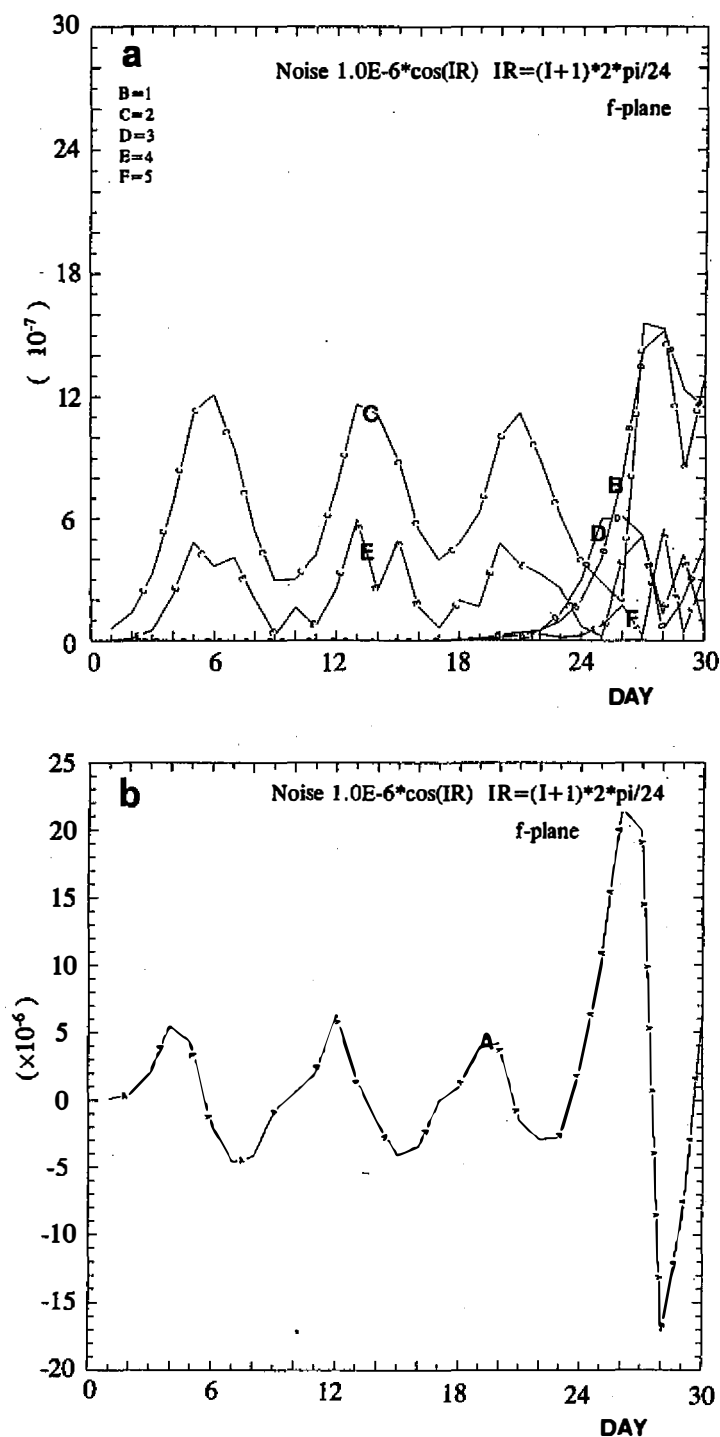


Fig. 14. Time series of spectral coefficients and the  $y$  averaged wave-mean energy conversion rate  $-\overline{u'v'} d\bar{u}/dy$ . The sudden breakup of the shear zone after three cycles of wave-mean flow energy exchange is obvious.

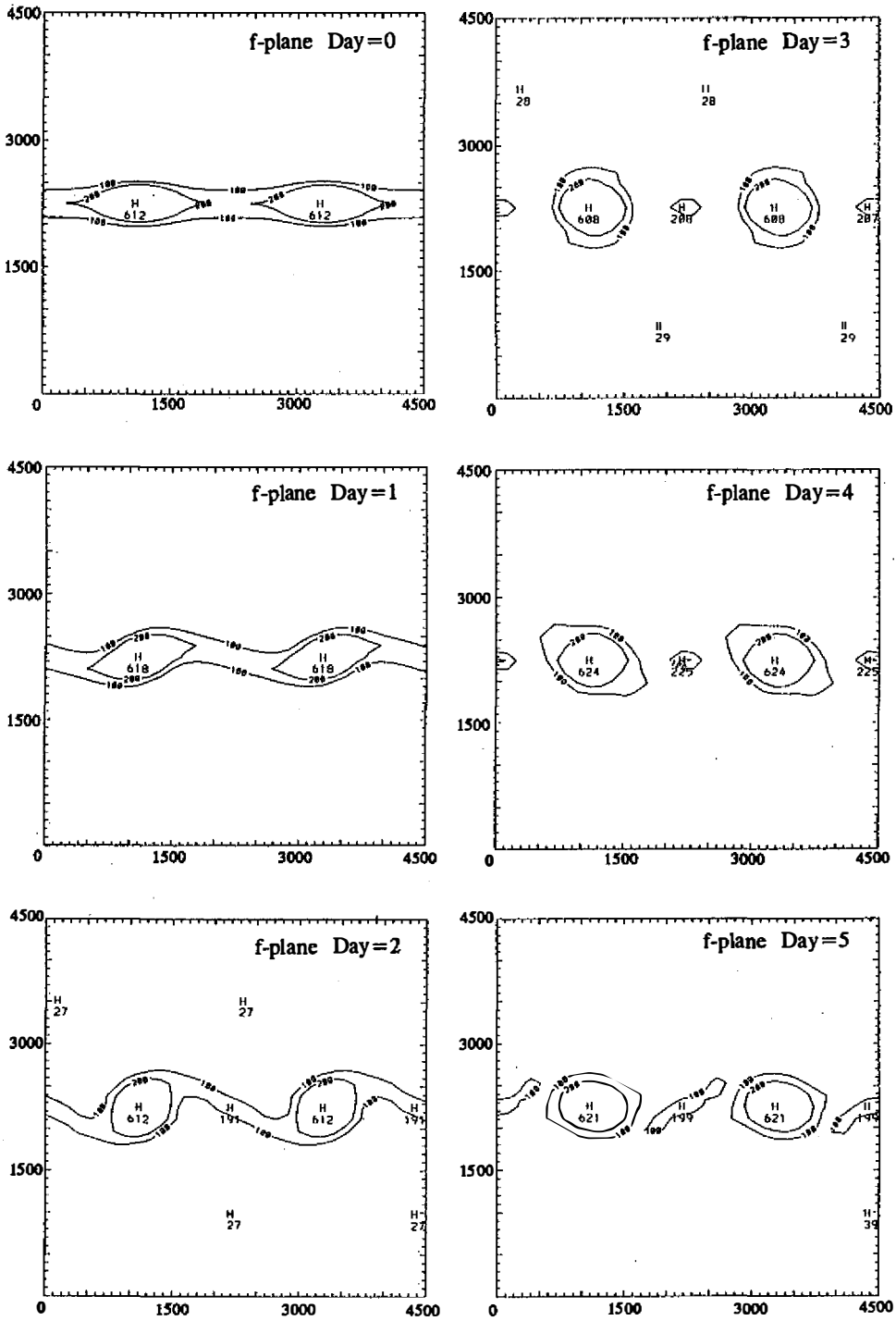


Fig. 15. The vorticity field in the physical space for the chaotic experiment on  $f$  plane from day 0 to day 17 with one day interval. No white noise is added in this experiment. Contours of vorticity in the unit of  $10^{-7} \text{ s}^{-1}$ .

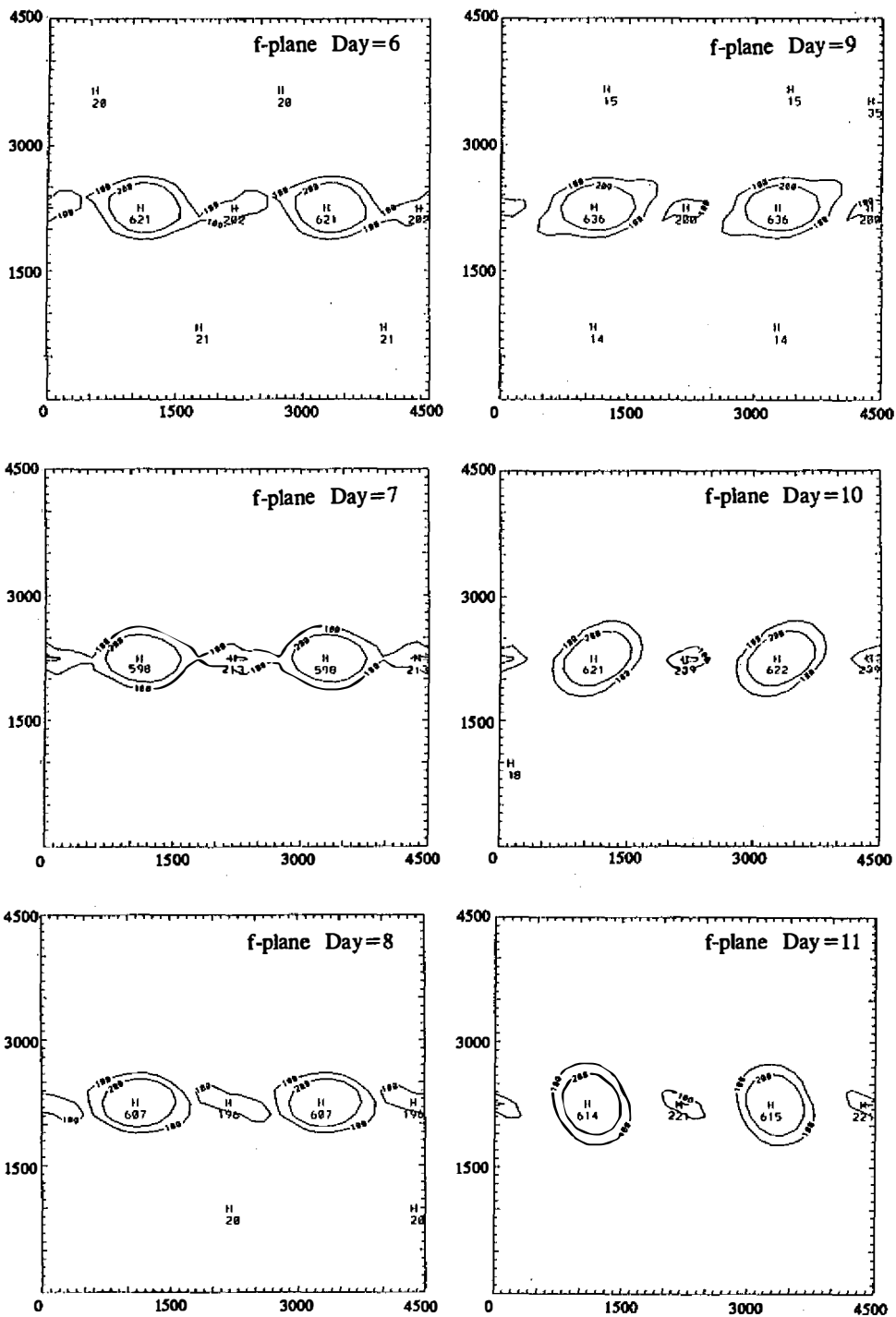


Fig. 15. (Continued.)

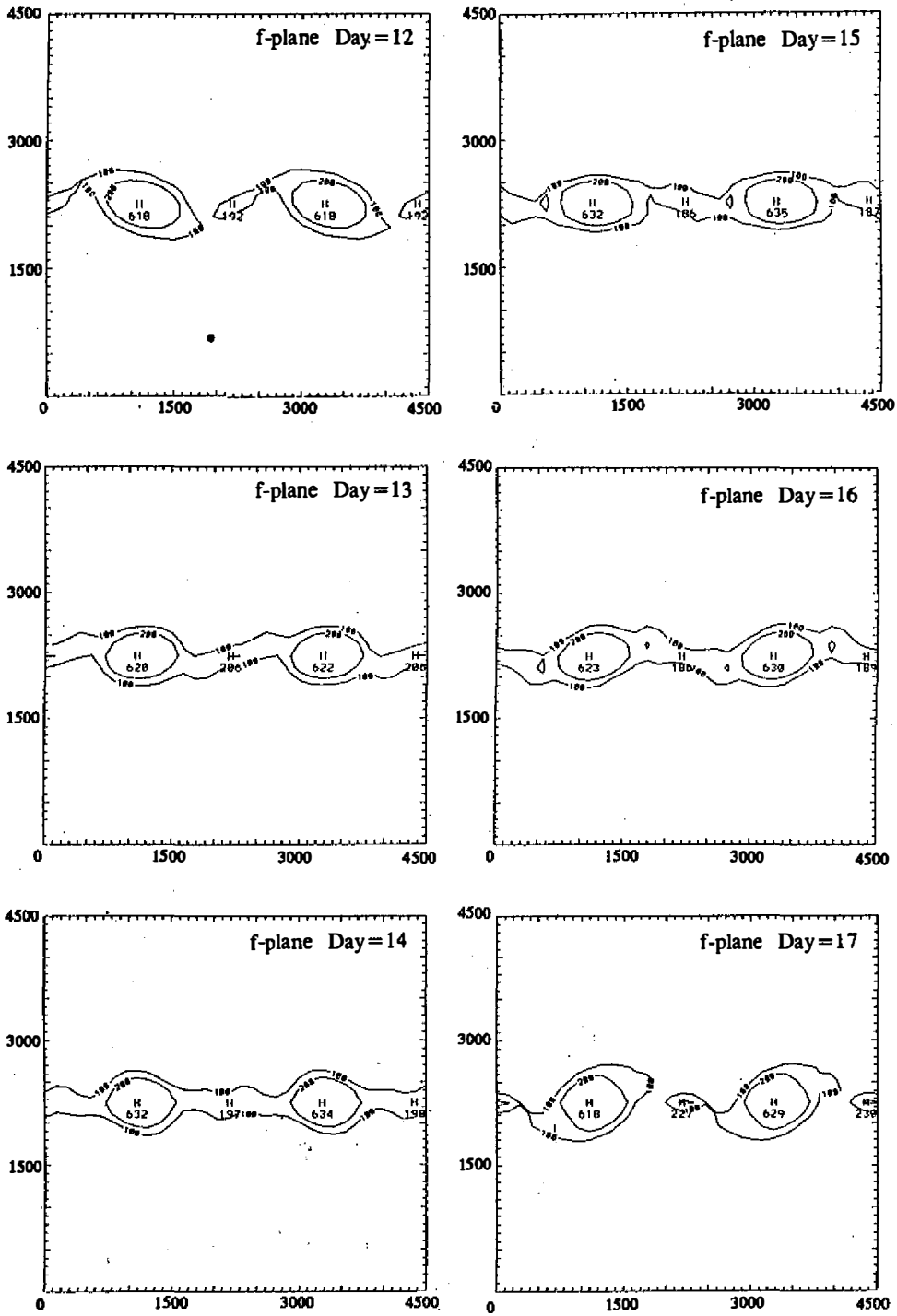


Fig. 15. (Continued.)

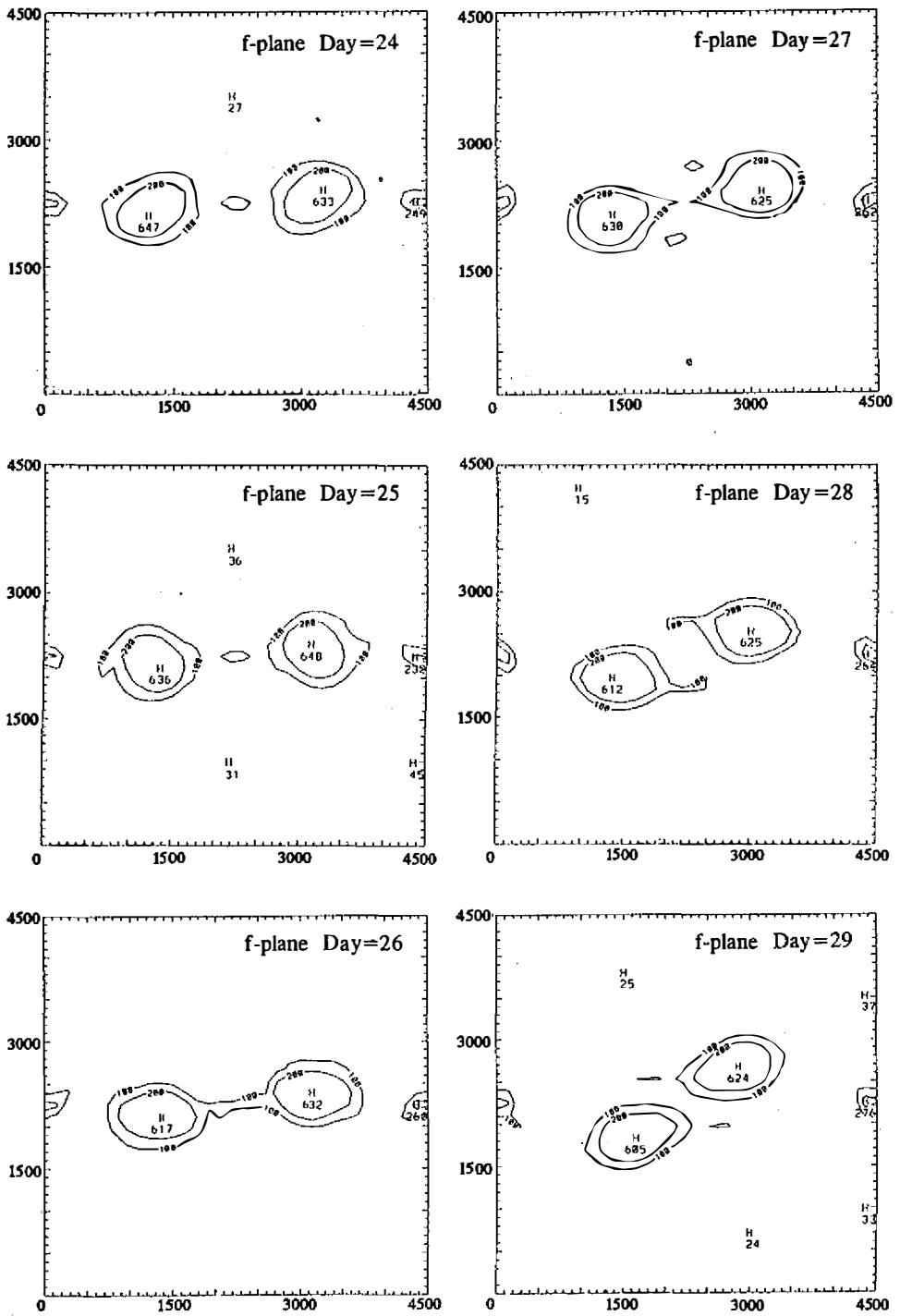


Fig. 16. Same as Figure 15 except for day 24 to 40 with one day intervals.



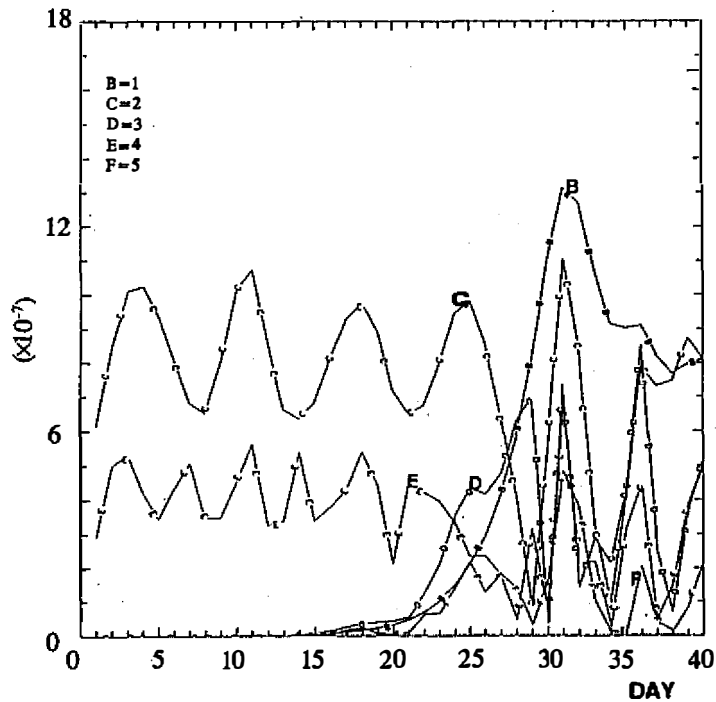


Fig. 17. Same as Figure 11 except for the chaotic experiment. The sudden breakup of shear zone after four cycles of wave-mean flow energy exchange is obvious.

## 6. SUMMARY AND CONCLUDING REMARKS

We present cases that contain a series of disturbances along the shear zone. In one case the wavy structures resemble the upshear tilted counter-propagating Rossby waves (vorticity gradient waves) on the edge of shear zones. In the other case the disturbances are elongated in the upshear sense as is required by barotropic instability. The horizontal shear in one case decreases after the series of disturbances grows. Since the scale involved is much smaller than the local Rossby radius of deformation, we hypothesize the relevance of barotropic instability.

Since we have not put the model spatial and time scales in the dimensionless form, the time and spatial unit in the model results should be interpreted with care. With the same initial  $\zeta$  on the  $f$  plane (which is of order  $10^{-4} \text{ s}^{-1}$  in our study), the 30 day integration on a 4500 km domain will yield exactly the same simulation sequence as the 3 day integration on a 450 km domain. Thus, according to the  $f$ -plane hyperbolic tangent simulations in section 4, the dominant wavelength of disturbance and the formation time can also be interpreted as 300 km (rather than 3000 km) and a couple of hours (rather than a couple of days), which agrees with the observations of Figures 2 and 3. However, as calculated in section 2, the dominant wavelength of 300 km barotropic disturbances in a hyperbolic type of wind shear profile requires a shear zone of 40 km, which is beyond the resolution of the present synoptic sounding system. Thus, we do not wish to imply that the growth of these series of disturbances is a purely barotropic case. Rather, we argue that the concentration of vorticity

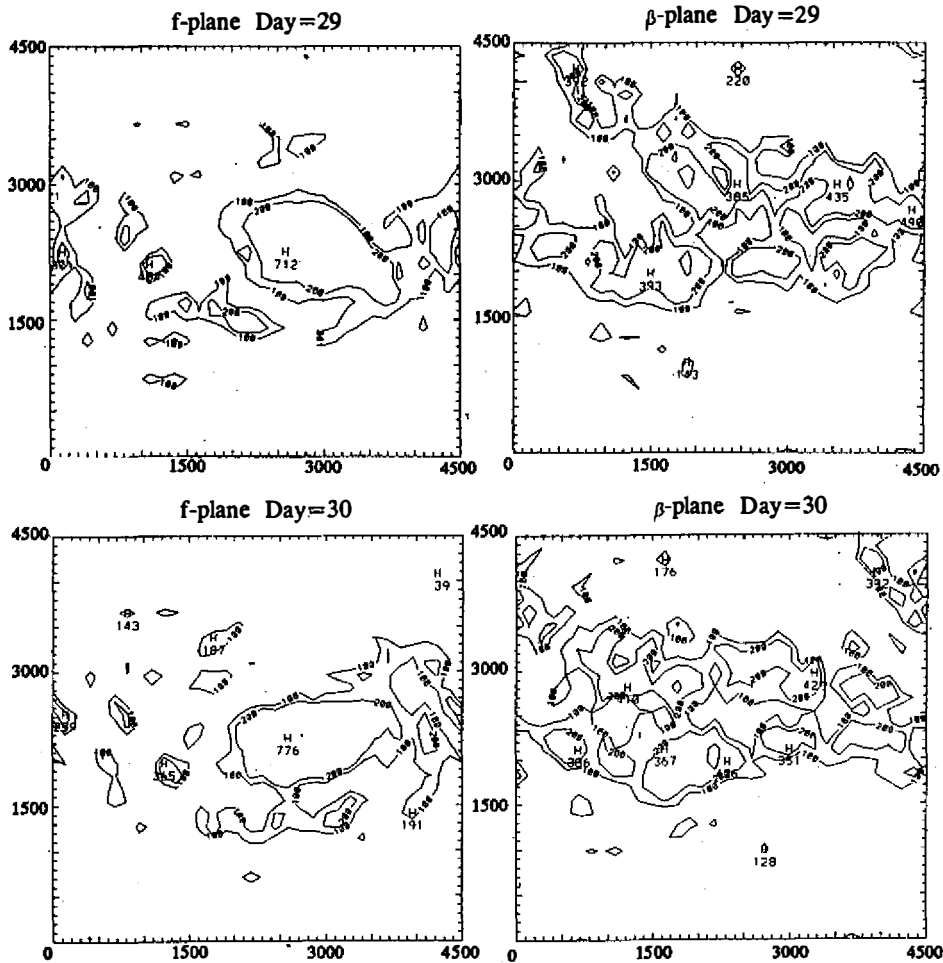


Fig. 18. The vorticity field in physical space in day 29 and 30 on  $f$  and  $\beta$  planes with random number set 13. The dominance of wave number 1 on  $f$  plane as compared to the small vortices scattered in northwest-southeast directions on the  $\beta$  plane.

and the follow-up vortex merging in the nonlinear evolution of barotropic instability can create a favorable localized environment within the shear zone for the moist baroclinic processes to operate. The intensity, shape and position of the preferred localized regions within the shear zone are unpredictable. Surely, the moist convection will lead to further modification or even enhancement of vorticity field (Schubert and Hack, 1983), which will greatly complicate the data analysis to identify the origin of the convective systems. The positive feedback between convection and the vorticity field in Mei-Yu frontogenesis was studied by Cho (1993). The Mei-Yu season contains a lot of complex phenomena. Without further analysis case by case (data may not even be available), we do not intend to suggest that barotropic instability plays a dominant role in every wind shear situation. Indeed, Moore's (1985) linear analysis on the conditional unstable atmosphere embedded in a shear

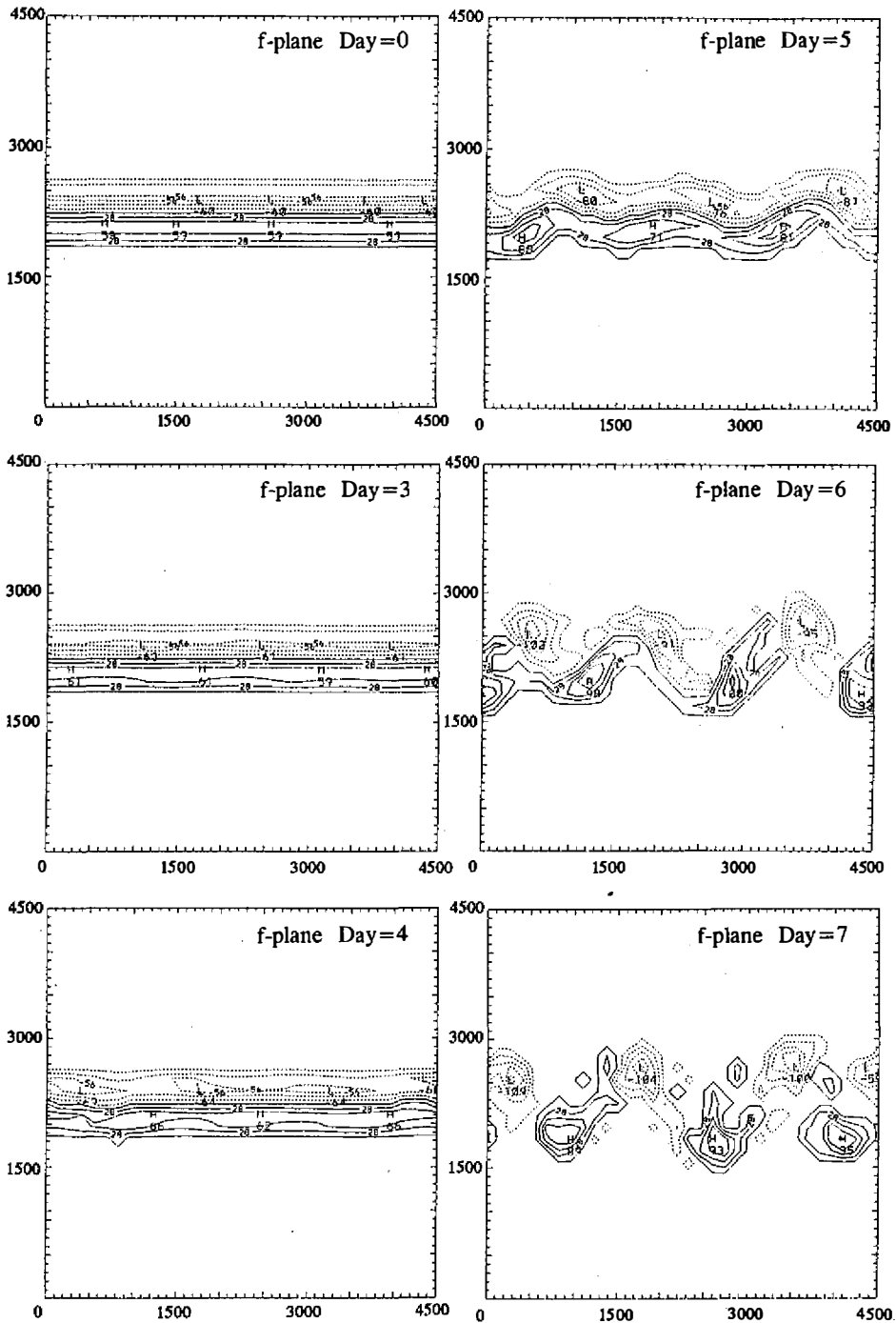


Fig. 19. The vorticity field in the physical space for the experiment with Bickerly jet as initial condition on  $f$  plane. Both fields in day 0 (initial condition), day 30 and day 3 to day 12 are shown. The contours of vorticity in the unit of  $10^{-7} \text{ s}^{-1}$ .

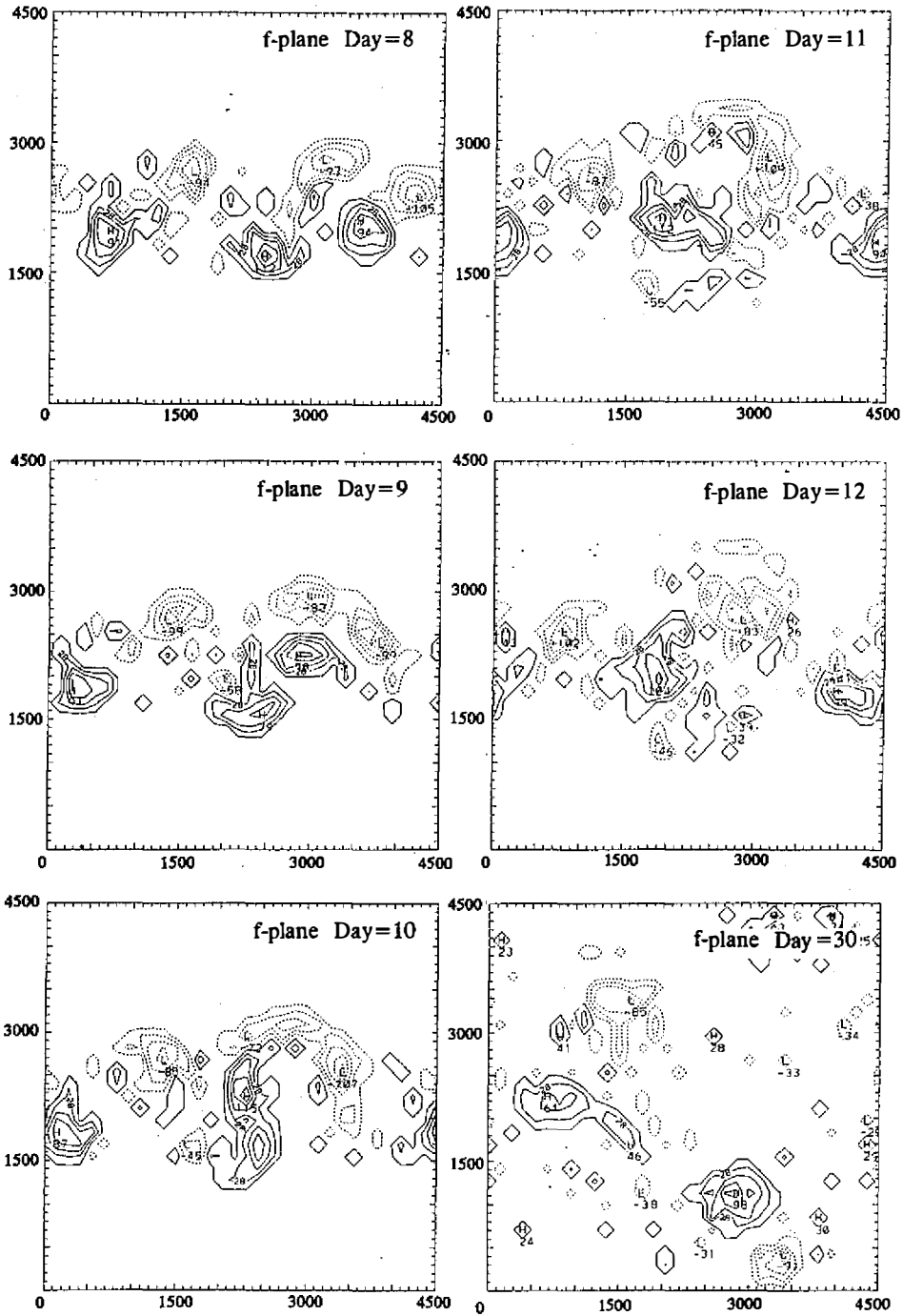


Fig. 19. (Continued.)

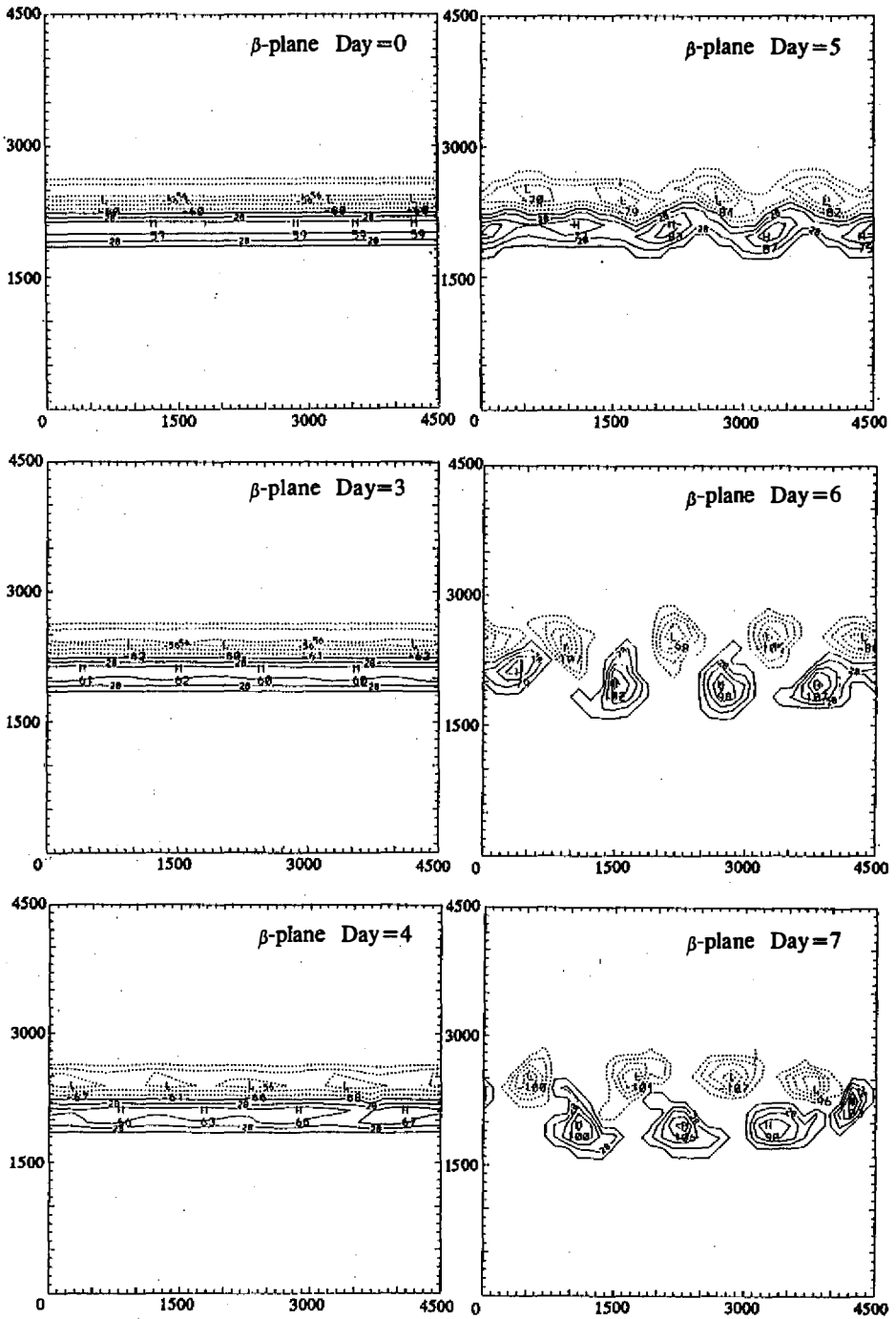


Fig. 20. Same as Figure 19 except on the  $\beta$  plane.

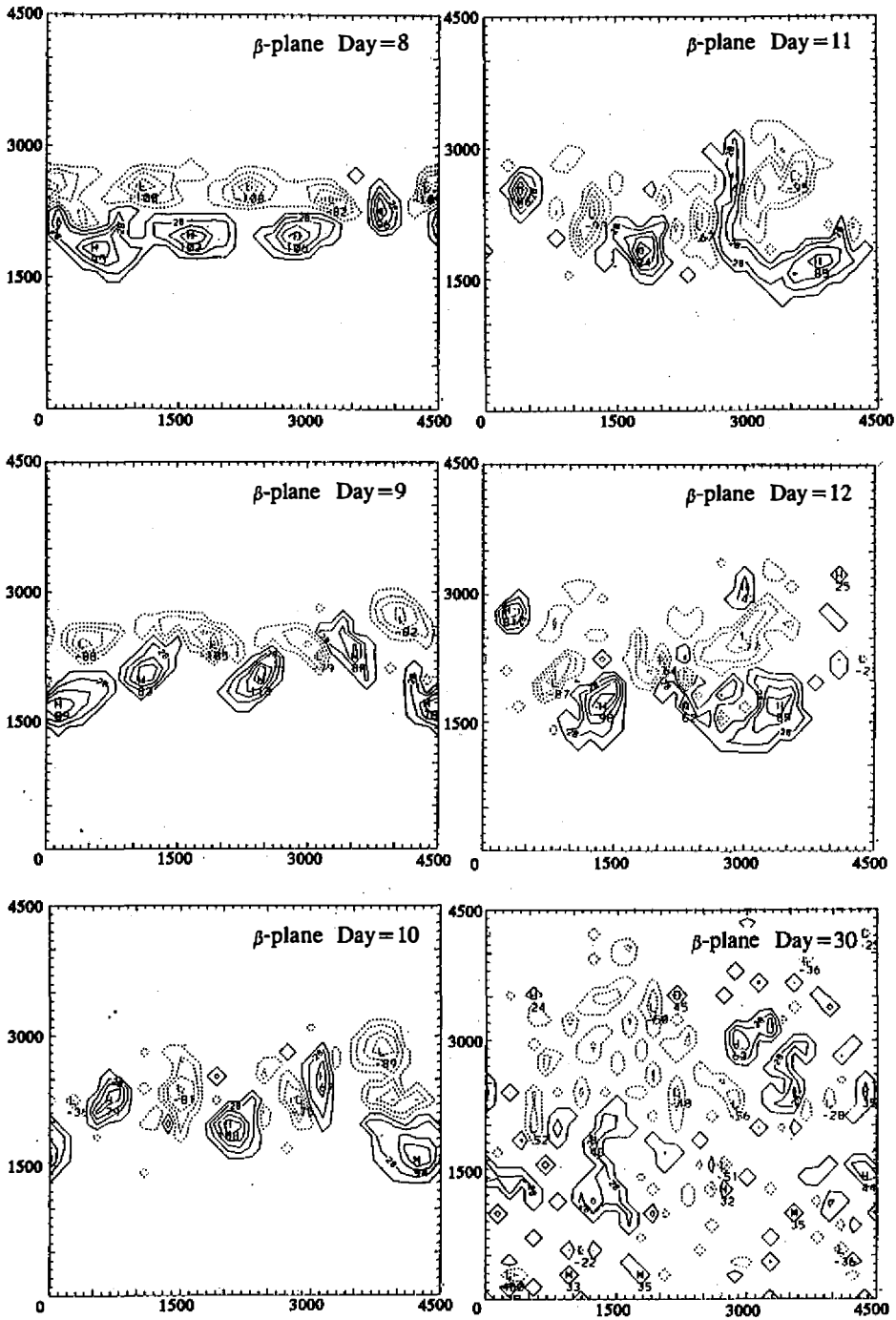


Fig. 20. (Continued.)

Easterly Jet, RAN(13), RAN(79)

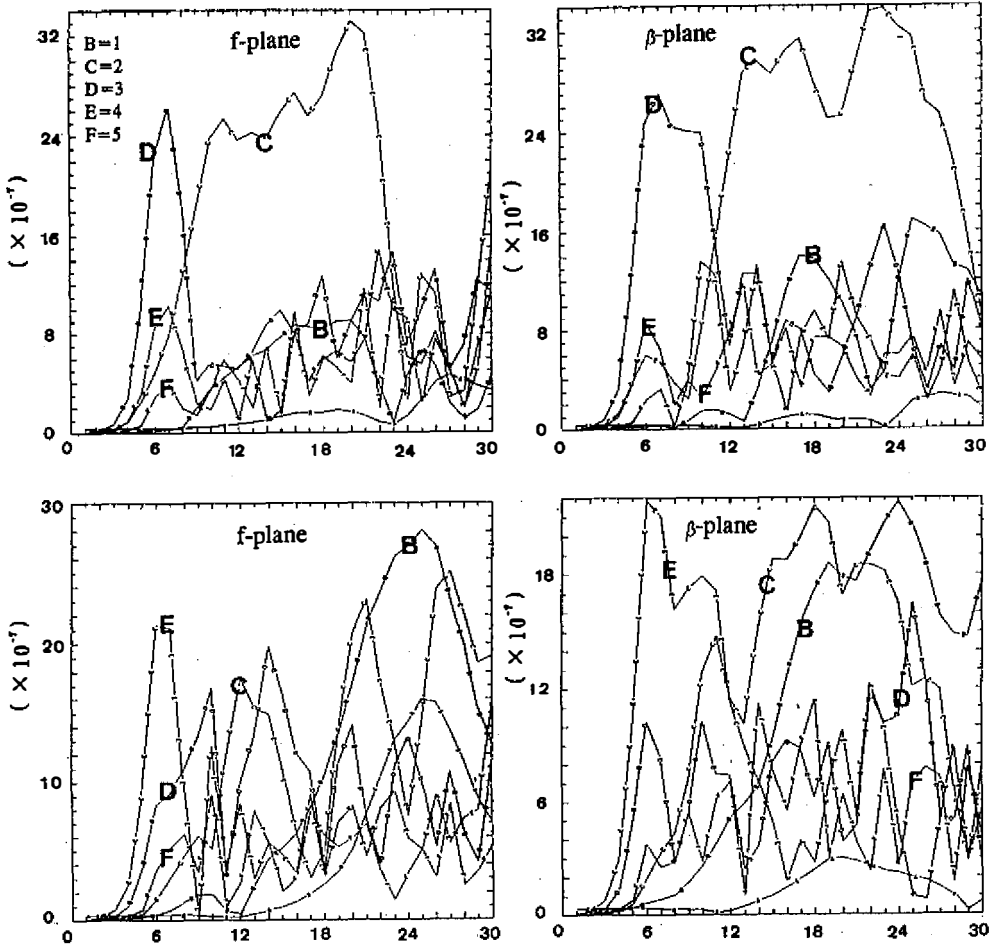


Fig. 21. Time series (up to day 30) of  $y$ -averaged spectral coefficients from wavenumber 1 to 5 for experiments with easterly Bickerly jet initial condition and different white noises on the  $f$  (left column) and  $\beta$  (right column) planes.

zone suggests that the horizontal shear may simply distort the shape of convection in the downshear orientation.

The nonlinear evolutions of barotropic instability are studied. We review the small and finite amplitude theories. Eigenvalues of ideal three and four region models are explored. A new Fourier Chebyshev nondivergent barotropic model is constructed. Using the initial value problem approach, we experiment on barotropic instability with a vorticity strip that either has a hyperbolic tangent or a Bickerly jet type of wind profile. We study the time evolution of the shear layers in terms of the formation of fundamental eddies and successive pairing or merging of eddies. The mutual intensification of counter-propagating Rossby waves (vorticity waves) across the strip, breakdown of the vorticity strip, the local concentration of vorticity and vortex merger processes are simulated. The dominant wavelength is well

predicted by linear analysis. In addition, we observe upshear tilted vortices with uneven sizes, in agreement with the satellite images. The local concentration of vorticity is stronger in the Bickerly jet case than that in the hyperbolic case. However, the vorticity concentration only occurs during the process of shear zone breakup. The later vortex merging will only affect the size of eddies but not the strength. Barotropic instability can be viewed as an efficient way to get vortex concentrated in a small region with the later vortex merging as a mean to enlarge the vortex sizes. Both processes give favorable conditions for the moist convection to grow (CISK mechanism).

As far as the nonlinear evolution of the vortex intensity, vortex shape and vortex positions are concerned, they are very sensitive to the initial background noise and model resolution. In other words, there is no predictability at all. However, the maximum growth rate and the dominant wavelength of the vortex are well predicted by linear analysis. The Bickerly jet seems to possess higher growth rate than the hyperbolic tangent case. Cases of chaotic behavior are observed in our simulations. The chaos contains a couple of wave-mean flow interaction cycles with the shear zone maintained and the sudden break up of the shear zone. In the thirty-day integration, the vortices on the  $\beta$  plane are less organized while they remain well organized on the  $f$  plane.

**Acknowledgments** The authors would like to thank Profs. Wayne Schubert, W.-Y. Sun and Terry Williams for helpful discussions. We also like to thank two anonymous reviewers' very careful review of our paper.

This work was supported by the Grants NSC 82-0202-M002-073 and NSC 83-0202-M002-058 from the National Research Council of Taiwan. The computing was performed at DEC workstation 5240 "Lanczos" at the Department of Atmospheric Sciences of National Taiwan University.

## REFERENCES

- Andrews, D. G., 1983: A conservation law for small amplitude quasi-geostrophic disturbances on a zonally asymmetric basic flow. *J. Atmos. Sci.*, **40**, 85-90.
- Andrews, D. G., J. R. Holton, and C. B. Leovy, 1987: *Middle Atmosphere Dynamics*. Academic Press, New York, 489pp.
- Arnol'd, V. I., 1965: Conditions for nonlinear stability of stationary plane curvilinear flows of an ideal fluid. *Dokl. Akad. Nauk. SSSR*, **162**, 975-978 (English translation: *Soviet Math.*, **6**, 773-777).
- Arnol'd, V. I., 1966: On an a priori estimate in the theory of hydrodynamical instability. *Izv. Vyssh. Uchibn. Zaved. Matematika*, **54**, no. 5, 3-5 (English translation: *American Math. Soc. Transl. Series 2*, **79**, 267-269).
- Charney, J. G., and M. E. Stern, 1962: On the stability of internal baroclinic jets in a rotating atmosphere. *J. Atmos. Sci.*, **19**, 159-172.
- Chen, G. T. J., 1992: Mesoscale features observed in the Taiwan Mei-Yu season. *J. Meteor. Soc. Japan*, **70**, 497-516.

- Chen, G. T. J., and C.-P. Chang, 1980: The structure and vorticity budget of an early summer monsoon trough (Mei-Yu) over southeastern China and Japan. *Mon. Wea. Rev.*, **108**, 942-953.
- Cho, H.-R., 1993: Convection and Mei-Yu front. Proceedings, International Workshop on Mesoscale Research and TAMEX Program Review, Taipei, 108-116.
- Crum, F. X., and D. E. Stevens, 1990: Barotropic instability with downstream variation and asymmetric cross-stream variations: Idealized calculations. *J. Atmos. Sci.*, **47**, 5-23.
- Drazin, P. G., and W. H. Reid, 1981: Hydrodynamic Stability. Cambridge Univ. Press, Cambridge, England.
- Eliassen, A., 1983: The Charney-Stern theorem on barotropic-baroclinic instability. *Pure Appl. Geophys.*, **121**, 563-572.
- Eliassen, E., B. Machenhauer, and E. Rasmussen, 1970: On a numerical method for integration of the hydrodynamical equations with a spectral representation of the horizontal fields. Report No. 2, Institut for Teoretisk Meteorologi, Kobenhavns Universitet, 35pp.
- Fulton, S. R., and W. H. Schubert, 1987: Chebyshev spectral methods for limited-area models. I: Model problem analysis. *Mon. Wea. Rev.*, **115**, 1940-1953.
- Gill, A. E., 1982: Atmosphere-Ocean Dynamics. Academic Press, 662pp.
- Gottlieb, D., and S. A. Orszag, 1977: Numerical Analysis of Spectral Methods. NSF-CBMS Monograph No. 26, NTIS No. AD-A056 922, Soc. Ind. and Appl. Math., Philadelphia, 172pp.
- Guinn, T. A., and W. H. Schubert, 1993: Hurricane spiral bands. *J. Atmos. Sci.*, **50**, 3380-3403.
- Haurwitz, B., 1949: The instability of wind discontinuities and shear zones in planetary atmospheres. *J. Meteor.*, **6**, 200-206.
- Haynes, P. H., 1988: Forced, dissipative generalizations of finite amplitude wave activity conservation relations for zonal and nonzonal basic flows. *J. Atmos. Sci.*, **45**, 2352-2362.
- Hoskins, B. J., M. E. McIntyre, and A. W. Robertson, 1985: On the use and significance of isentropic potential vorticity maps. *Quart. J. Roy. Meteor. Soc.*, **111**, 877-946.
- Kuo, H.-C., and W. H. Schubert, 1988: Stability of cloud-topped boundary layers. *Quart. J. Roy. Meteor. Soc.*, **114**, 887-916.
- Kuo, H.-L., 1949: Dynamical instability of two-dimensional nondivergent flow in a barotropic atmosphere. *J. Meteor.*, **6**, 105-122.
- Lesieur, M., C. Staquet, P. LeRoy and P. Comte, 1988: The mixing layer and its coherence examined from the point of view of two-dimensional turbulence. *J. Fluid Mech.*, **192**, 511-534.
- Magnusdottir, G., and W. H. Schubert, 1990: On the generalization of semigeostrophic theory to the  $\beta$ -plane. *J. Atmos. Sci.*, **47**, 1714-1720.
- Magnusdottir, G., and W. H. Schubert, 1991: Semigeostrophic theory on the hemisphere. *J. Atmos. Sci.*, **48**, 1449-1456.

- McIntyre, M. E., and T. G. Shepherd, 1987: An exact local conservation theorem for finite-amplitude disturbances to non-parallel shear flows, with remarks on Hamiltonian structure and on Arnol'd's stability theorems. *J. Fluid Mech.*, **181**, 527-565.
- Moore, G. W. K., 1985: The organization of convection in narrow cold-frontal rainbands. *J. Atmos. Sci.*, **42**, 1777-1791.
- Orszag, S. A., 1970: Transform method for the calculation of vector-coupled sums: Application to the spectral form of the vorticity equation. *J. Atmos. Sci.*, **27**, 890-895.
- Rayleigh, J. W. S., 1945: *The Theory of Sound, Volume II*. Dover Publications, New York (reprint of the 1894 edition), 504pp.
- Ripa, P., 1983: General stability conditions for zonal flows in a one-layer model on the beta-plane or the sphere. *J. Fluid Mech.*, **126**, 463-487.
- Ripa, P., 1991: General stability conditions for a multi-layer model. *J. Fluid Mech.*, **222**, 119-137.
- Schubert, W. H., P. E. Ciesielski, and K. W. Harding, 1992: Dynamics of the Australian summer monsoon. Atmospheric Science Paper No. 492, Univ. Colorado State, 48pp.
- Schubert, W. H., and J. J. Hack, 1983: Inertial stability and tropical cyclone development. *J. Atmos. Sci.*, **39**, 1687-1697.
- Shepherd, T. G., 1988a: Rigorous bounds on the nonlinear saturation of instabilities to parallel shear flows. *J. Fluid Mech.*, **196**, 291-322.
- Shepherd, T. G., 1988b: Nonlinear saturation of baroclinic instability. Part I: The two-layer model. *J. Atmos. Sci.*, **45**, 2014-2025.
- Shepherd, T. G., 1989: Nonlinear saturation of baroclinic instability. Part II: Continuously stratified fluid. *J. Atmos. Sci.*, **46**, 888-907.
- Sun, W.-Y., and Y.-L. Chang, 1992: Barotropic instability of modified hyper-tangent shear flows. *Beitr. Phys. Atmos.*, **65**, 193-210.
- Williams R. T., H. Lim and C. P. Chang, 1984: Nonlinear and linear effects in an easterly jet with downstream variation. *J. Atmos. Sci.*, **41**, 621-636.